A well-balanced scheme for the shallow-water equations with topography and Manning friction.

Victor Michel-Dansac, Christophe Berthon, Stéphane Clain, Françoise Foucher

A well-balanced scheme for the shallow-water equations with topography and Manning friction.

Victor Michel-Dansac[a,*], Christophe Berthon[a], Stéphane Clain[b], Françoise Foucher[a,c]

[a] *Laboratoire de Mathématiques Jean Leray, CNRS UMR 6629, Université de Nantes, 2 rue de la Houssinière, BP 92208, 44322 Nantes Cedex 3, France*
[b] *Centre of Mathematics, Minho University, Campus de Gualtar - 4710-057 Braga, Portugal*
[c] *École Centrale de Nantes, 1 rue de La Noë, BP 92101 44321 Nantes Cedex 3, France*

Abstract

We consider the shallow-water equations with Manning friction and topography source terms. The main purpose of this work concerns the derivation of a non-negativity preserving and well-balanced scheme that approximates solutions of the system and preserves the associated steady states, including the moving ones. In addition, the scheme has to deal with vanishing water heights and transitions between wet and dry areas. To address such issues, a particular attention is paid to the study of the steady states related to the friction source term. Then, a Godunov-type scheme is obtained by using a relevant average of the source terms in order to enforce the required well-balance property. An implicit treatment of both topography and friction source terms is also exhibited to improve the scheme while dealing with vanishing water heights. A second-order well-balanced MUSCL extension is designed, as well as an extension for the two-dimensional case. Numerical experiments are performed in order to highlight the properties of the scheme.

Keywords: shallow-water equations, Manning friction, Godunov-type schemes, well-balanced schemes, moving steady states
2000 MSC: 65M08, 65M12

1. Introduction

The goal of this paper is to derive a numerical scheme to approximate the solutions of the shallow-water equations with topography and Manning friction. The Manning friction was introduced in [34] (see also [15] for an overview of

*Corresponding author
Email addresses: victor.michel-dansac@univ-nantes.fr (Victor Michel-Dansac), christophe.berthon@univ-nantes.fr (Christophe Berthon), clain@math.uminho.pt (Stéphane Clain), francoise.foucher@ec-nantes.fr (Françoise Foucher)

other friction models, and [9, 10, 11] for related works). The equations of interest consist in the following system:

$$\begin{cases} \partial_t h + \partial_x q &= 0, \\ \partial_t q + \partial_x \left(\dfrac{q^2}{h} + \dfrac{1}{2} g h^2 \right) &= -gh\partial_x Z - \dfrac{kq|q|}{h^\eta}. \end{cases} \tag{1.1}$$

This system is used to model the flow of water in a one-dimensional channel, with a non-flat bottom that applies a friction force on the water. The variables involved in this model are the non-negative water height $h(x, y)$ and the depth-averaged discharge of the water $q(x, t)$. The known quantities are the shape of the channel bottom $Z(x)$, the gravity constant g, the Manning friction coefficient k and a parameter η, equal to $7/3$. We also define the velocity u of the water, such that $q = hu$.

We define the admissible states space by

$$\Omega = \left\{ W = {}^t(h, q) \in \mathbb{R}^2 \ ; \ h \geq 0, \, q \in \mathbb{R} \right\}.$$

Let us note that the water height may vanish, which accounts for dry areas. By convention, we impose $u = 0$ as soon as $h = 0$.

In order to shorten the notations, the system (1.1) is rewritten under a simpler form, as follows:

$$\partial_t W + \partial_x f(W) = s(W), \quad W \in \Omega, \tag{1.2}$$

where

$$W = \begin{pmatrix} h \\ q \end{pmatrix}, \quad f(W) = \begin{pmatrix} q \\ \dfrac{q^2}{h} + \dfrac{1}{2} g h^2 \end{pmatrix}, \quad s(W) = \begin{pmatrix} 0 \\ -gh\partial_x Z - \dfrac{kq|q|}{h^\eta} \end{pmatrix}. \tag{1.3}$$

Omitting the source terms, the homogeneous system deriving from (1.1) is a hyperbolic system. Its characteristic velocities are given by $u - c$ and $u + c$ (see [10, 20, 29] for instance), where c is the sound speed, defined as follows:

$$c = \sqrt{gh}. \tag{1.4}$$

The main focus on this paper lies in the study of the solutions of (1.2) that satisfy $\partial_t W = 0$. Such solutions are called *steady state solutions*. With vanishing partial derivatives in time in (1.1), we get:

$$\begin{cases} \partial_x q &= 0, \\ \partial_x \left(\dfrac{q^2}{h} + \dfrac{1}{2} g h^2 \right) &= -gh\partial_x Z - \dfrac{kq|q|}{h^\eta}. \end{cases} \tag{1.5}$$

We immediately obtain that, as per the first equation, the discharge q must be uniform. From now on, we denote this uniform discharge as follows:

$$q = q_0. \tag{1.6}$$

Using q_0 within the second equation of (1.5) yields:

$$\partial_x \left(\frac{q_0^2}{h} + \frac{1}{2} g h^2 \right) = -gh\partial_x Z - \frac{k q_0 |q_0|}{h^\eta}. \tag{1.7}$$

The solution of the nonlinear ordinary differential equation (1.7) is the water height h for a steady state with uniform discharge q_0. For a general topography and a nonzero friction contribution, if $q_0 \neq 0$, we cannot solve this equation to obtain an analytical expression for h. Thus, we will focus on specific cases; namely, the steady states at rest, and the steady states with topography or friction only.

The most important and most extensively studied steady state of the shallow-water equations is the *lake at rest* steady state (see for instance the non-exhaustive list [2, 8, 10, 12, 19, 24]). The lake at rest is obtained by assuming that the water is at rest, i.e. $q_0 = 0$. Thus, this steady state is defined as follows:

$$\left\{ \begin{array}{rcl} q & = & 0, \\ h + Z & = & \text{cst}\,. \end{array} \right. \tag{1.8}$$

The importance of this steady state has led to the derivation of many schemes ensuring that the lake at rest is preserved. For instance, in [3, 24], the authors introduced the notion of a *well-balanced scheme*, that is to say a scheme that preserves some or all the steady states. Next, the well-balance approach was extended to nonlinear systems in [21]. The techniques from [21] were then simplified in [1], to obtain the hydrostatic reconstruction (see also [8, 17, 18, 27, 31, 32, 36]).

Now, let us consider a vanishing friction source term (i.e. $k = 0$) without being at rest (i.e. $q_0 \neq 0$). From (1.7), we get the *moving steady states*, governed by

$$\partial_x \left(\frac{q_0^2}{h} + \frac{1}{2} g h^2 \right) = -gh\partial_x Z. \tag{1.9}$$

The equation (1.9) that defines the moving steady states is known to be harder to satisfy at the discrete level than the lake at rest. Indeed, the lake at rest explicitly yields h with respect the the known quantity Z, while the water height is given by the nonlinear ODE (1.9) in the case of the moving steady states. Such steady states have been studied in the past, for instance in [23], where the authors define some specific moving steady states and use them to test the accuracy of non-well-balanced schemes. Then, in [21], the author introduced the notion of fully well-balanced schemes, able to preserve every steady state, and designed such a scheme. This approach was extended in [4], where the authors derive a fully well-balanced and entropy-stable Godunov-type scheme, based on the resolution of a Bernoulli-type equation. Since this equation is difficult to solve, the authors of [35] have proposed a fully well-balanced Godunov-type scheme that uses a linearization of the Bernoulli-type equation. In addition, high-order techniques were developed to ensure a very precise approximation of the moving steady states (see for instance [38, 39, 44, 45]).

Let us now assume a flat topography and a nonzero discharge. The steady states governed by the friction source term are given as follows:

$$\partial_x \left(\frac{q_0^2}{h} + \frac{1}{2} g h^2 \right) = -\frac{k q_0 |q_0|}{h^\eta}. \tag{1.10}$$

Some research has been devoted to Manning friction terms (for instance, see [15, 9]), but these works do not focus on steady states and the resulting schemes are not well-balanced.

In the present paper, we exhibit smooth steady solutions of (1.10) and propose a well-balanced scheme, according to the lake at rest (1.8), to the moving steady states (1.9), and to the dominant friction steady states (1.10). This scheme will be derived in order to satisfy some essential properties, namely the exact preservation of all the steady states for the system (1.1) with topography or friction and the preservation of the non-negativity of the water height. In addition, the scheme will be designed to model transitions between wet areas, where $h \neq 0$ and dry areas, where $h = 0$.

The paper is organized as follows. First, in Section 2, we study smooth steady states for the shallow-water equations with friction over a flat bottom. Then, in Section 3, we develop a Godunov-type scheme that is well-balanced for the system Section 1.1. In this section, we first recall some generalities on Godunov-type schemes, then we derive the well-balanced scheme, according to the friction steady states. Afterwards, in Section 4, we extend this scheme to be well-balanced for both the topography and the friction source terms. In addition, in this section, we prove the non-negativity preservation. Then, in Section 5, we propose an implicitation of the source terms contribution, designed to deal with transitions between wet and dry areas. The scheme is then extended in Section 6 to be second-order accurate. This extension breaks the well-balance property, but we show a convex combination technique that allows the recovery of this essential property. Finally, in Section 7, we propose three kinds numerical experiments, namely well-balance assessments, dam-break simulations, and two dimensional simulations. The paper is concluded in Section 8.

2. Steady states characterization

This section is devoted to studying the steady states coming from the friction source term, given by (1.5) with a flat topography ($Z = \text{cst}$), or equivalently by (1.10). Recall that, for steady states and after (1.6), the discharge $q = q_0$ is uniform throughout the domain. Here, we assume $q_0 \neq 0$. Indeed, we assume that the friction contribution vanishes as soon as the discharge is equal to zero. We rewrite (1.10) under the form:

$$q_0^2 \, \partial_x \frac{1}{h} + \frac{g}{2} \, \partial_x h^2 = -\frac{k q_0 |q_0|}{h^\eta}. \tag{2.1}$$

We are looking for smooth solutions $h(x) > 0$ of the equation (2.1). As a first step, we integrate this equation. Multiplying by h^η provides:

$$-\frac{q_0^2}{\eta-1}\,\partial_x h^{\eta-1} + \frac{g}{\eta+2}\,\partial_x h^{\eta+2} = -kq_0|q_0|. \tag{2.2}$$

Let us consider $x_0 \in \mathbb{R}$ as an arbitrary reference point, and introduce the initial condition $h(x_0) = h_0$. For all $x \in \mathbb{R}$, we integrate (2.2) over (x_0, x), to get

$$-\frac{q_0^2}{\eta-1}\left(h^{\eta-1} - h_0^{\eta-1}\right) + \frac{g}{\eta+2}\left(h^{\eta+2} - h_0^{\eta+2}\right) + kq_0|q_0|\,(x - x_0) = 0. \tag{2.3}$$

To shorten the notations, we rewrite (2.3) under the following form:

$$\xi(h; x, h_0, q_0, x_0) = 0, \tag{2.4}$$

where we have set

$$\begin{aligned}\xi(h; x, h_0, q_0, x_0) = &-\frac{q_0^2}{\eta-1}\left(h^{\eta-1} - h_0^{\eta-1}\right) + \frac{g}{\eta+2}\left(h^{\eta+2} - h_0^{\eta+2}\right)\\ &+ kq_0|q_0|\,(x - x_0)\,.\end{aligned} \tag{2.5}$$

We consider x a parameter so that (2.4) is an equation to characterize $h := h(x)$. In order to exhibit such solutions, we first study ξ with a fixed $x \in \mathbb{R}$. The derivative of ξ with respect to h is given by

$$\frac{\partial \xi}{\partial h}(h; x, h_0, q_0, x_0) = gh^{\eta-2}\left(-\frac{q_0^2}{g} + h^3\right).$$

Let us define a critical water height h_c, such that $\dfrac{\partial \xi}{\partial h}(h_c; x, h_0, q_0, x_0) = 0$, as follows:

$$h_c = \left(\frac{q_0^2}{g}\right)^{1/3}. \tag{2.6}$$

We easily obtain that the function $h \mapsto \xi(h; x, h_0, q_0, x_0)$ is strictly increasing on $(h_c, +\infty)$, while it is strictly decreasing on $(0, h_c)$. As a consequence, it admits a unique minimum in $(0, +\infty)$, and this minimum is reached for $h = h_c$.

Now, we evaluate the sign of ξ. After straightforward computations, the following limits are proven to be satisfied by ξ:

- $\lim\limits_{h \to +\infty} \xi(h; x, h_0, q_0, x_0) = +\infty$,
- $\lim\limits_{h \to 0^+} \xi(h; x, h_0, q_0, x_0) = \xi_\ell(x)$,

where we have set

$$\xi_\ell(x) = gh_0^{\eta-1}\left(\frac{h_c^3}{\eta-1} - \frac{h_0^3}{\eta+2}\right) + kq_0|q_0|(x - x_0).$$

Note that ξ_ℓ is finite. Moreover, let us introduce

$$\xi_c(x) := \xi(h_c; x, h_0, q_0, x_0).$$

We note that

$$\xi_c(x) = \xi_\ell(x) - \frac{3gh_c^{\eta+2}}{(\eta-1)(\eta+2)} < \xi_\ell(x).$$

Equipped with these new notations and these properties of ξ, we state the following result.

Lemma 1. *Assume $h > 0$ and $q_0 \neq 0$. Thus, $h_c > 0$ according to (2.6).*

(i) If $\xi_\ell(x) < 0$, then the equation (2.4) admits a unique solution $h^{sub}(x)$. Moreover, this solution belongs to $(h_c, +\infty)$.

(ii) If $\xi_\ell(x) > 0$ and $\xi_c(x) > 0$, then there is no solution to the equation (2.4).

(iii) If $\xi_\ell(x) > 0$ and $\xi_c(x) < 0$, then the equation (2.4) admits two solutions, $h^{sup}(x)$ and $h^{sub}(x)$. One solution, $h^{sup}(x)$, stays within $(0, h_c)$, while the second one, $h^{sub}(x)$, is in $(h_c, +\infty)$. If $\xi_c(x) = 0$, the equation (2.4) admits h_c as a unique double solution.

Proof. To establish *(i)*, we use that $h \mapsto \xi(h; x, h_0, q_0, x_0)$ is strictly increasing on $(h_c, +\infty)$ and that $\xi_c(x) < \xi_\ell(x) < 0$, to deduce that the equation (2.4) admits a unique solution, which belongs to $(h_c, +\infty)$.

Next, we turn to proving *(ii)*. If $\xi_c(x) > 0$, since ξ reaches its unique minimum $\xi_c(x)$ for $h = h_c$, it is immediate that there is no solution to the equation (2.4).

Finally, concerning *(iii)*, we assume that $\xi_\ell(x) > 0$ and $\xi_c(x) < 0$. The monotonicity properties of ξ allow the immediate conclusion that the equation (2.4) admits two solutions. One solution stays within $(0, h_c)$ and corresponds to a supercritical state, while the second one is in $(h_c, +\infty)$ and provides a subcritical state. Moreover, if $\xi_c(x) = 0$, the equation (2.4) admits a double root, $h = h_c$.

The proof is thus achieved. □

Remark 1. Arguing the definition of the Froude number $\mathrm{Fr} = u/c$ (where c is the sound speed, defined by (1.4)), we obtain for steady states $\mathrm{Fr} = q_0/\sqrt{gh^3}$. Therefore, it is clear that $h > h_c$ (resp. $h < h_c$) corresponds to $\mathrm{Fr} < 1$ (resp. $\mathrm{Fr} > 1$), i.e. to a subcritical (resp. supercritical) flow. Thus, the solution h of (2.4) that lies in $(0, h_c]$ will henceforth be called the *supercritical branch*, while the solution of of (2.4) that lies in $[h_c, +\infty)$ will be called the *subcritical branch*.

Remark 2. Note that the case $\xi_\ell(x) = 0$ implies that $h = 0$ is a solution of the equation (2.4). However, this equation has been obtained using the positivity of h: therefore, $h = 0$ is not a valid solution of (2.4).

Now, we study the solutions h of (2.4) as functions of x. As a first step, we evaluate the monotonicity of h. To this end, we exhibit the derivative of h with respect to x by considering (2.2), which writes

$$\left(-q_0^2 h^{\eta-2} + g h^{\eta+1}\right) h'(x) = -k q_0 |q_0|.$$

Since $q_0^2 = g h_c^3$ from (2.6), we immediately obtain

$$g h^{\eta+1} \left(1 - \frac{h_c^3}{h^3}\right) h'(x) = -k q_0 |q_0|.$$

As a consequence, the sign of $h'(x)$ coincides with the sign of $q_0(h_c - h(x))$. Note that both $\xi_\ell(x)$ and $\xi_c(x)$ are linear in x, and $\xi_c(x) < \xi_\ell(x)$. Both of these quantities are thus linear functions of x, of slope $k q_0 |q_0|$, and are strictly monotonic in x. Therefore, there exists a unique x_u such that $\xi_\ell(x) = 0$, and a unique $x_c \neq x_u$ such that $\xi_c(x) = 0$. Thus, by Lemma 1, if there exists a solution $h(x)$ of the equation (2.4), it is either within $(0, h_c]$ or within $[h_c, +\infty)$, for all x where such a solution exists. Therefore, the sign of $h'(x)$ is constant, and h is strictly monotonic. As a consequence, h^{sub} and h^{sup} are bijective on their respective domains, since they are continuous and strictly monotonic.

These solutions are displayed in Figure 1. For the sake of simplicity, this figure has been obtained assuming that $h_0 = h_c$ (and thus $x_0 = x_c$) and that $q_0 < 0$.

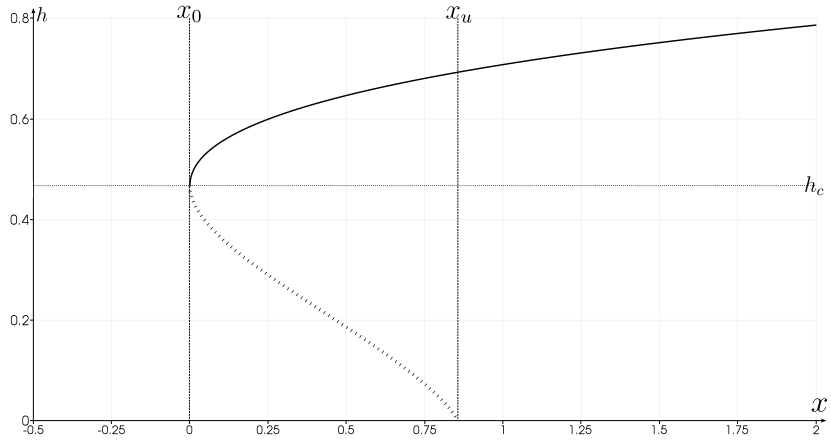

Figure 1: Solutions of (2.4) with $q_0 = -1$ and $x_0 = x_c = 0$, obtained by using Newton's method. The solid line is the *subcritical branch* (the increasing solution) and the dotted line is the *supercritical branch* (the decreasing solution).

As a consequence, we have obtained the general form of steady state solutions for the shallow-water equations (1.1) with friction and flat topography, respectively given by the subcritical and supercritical branches. However, the subcritical and supercritical branches that are solution to (2.4) are parametrized by the choice of the initial conditions x_0 and h_0.

3. A well-balanced scheme for a the shallow-water equations with friction

Equipped with the steady states, we now derive a numerical scheme able to exactly capture such essential solutions. We begin by recalling the construction of a Godunov-type scheme that uses a two-state approximate Riemann solver [25] (see also [10, 41]). The Godunov-type scheme is then adapted to the shallow-water equations with the friction source term. The purpose of this extension is to preserve the steady states presented in the previous section.

3.1. Generalities on Godunov-type schemes

First, we introduce the discretization of the space and time domain $\mathbb{R} \times \mathbb{R}^+$. Let Δx be the space step, assumed to be constant, and Δt the time step. The space discretization consists in cells $(x_{i-\frac{1}{2}}, x_{i+\frac{1}{2}})$, for all $i \in \mathbb{Z}$. The solution $W(x,t)$ of (1.2) is approximated by W_i^n at some time t^n and in cell $(x_{i-\frac{1}{2}}, x_{i+\frac{1}{2}})$. We suppose that this piecewise constant approximation of $W(x,t)$, here denoted $W^\Delta(x,t^n)$, is known at time t^n for all cells in the space domain. We now evolve $W^\Delta(x,t^n)$ in time, which consists in nothing but the solution of the following Riemann problem juxtaposition, defined for all $i \in Z$ and all x in two consecutive cells:

$$\begin{cases} \partial_t W + \partial_x f(W) = s(W), \\ W(x,t^n) = \begin{cases} W_i^n \text{ if } x < x_{i+\frac{1}{2}}, \\ W_{i+1}^n \text{ if } x > x_{i+\frac{1}{2}}. \end{cases} \end{cases} \tag{3.1}$$

From now on, let us emphasize that the consecutive Riemann solutions do not interact as long as t is small enough. Since an exact solution to (3.1) is difficult to determine, we suggest to consider an *approximate Riemann solver* to obtain an estimate of the unknown solution. We adopt a two-state approximate Riemann solver, illustrated by Figure 2 and defined as follows:

$$\widetilde{W}\left(\frac{x}{t}; W_L, W_R\right) = \begin{cases} W_L & \text{if } x/t < \lambda_L, \\ W_L^* & \text{if } \lambda_L < x/t < 0, \\ W_R^* & \text{if } 0 < x/t < \lambda_R, \\ W_R & \text{if } x/t > \lambda_R, \end{cases} \tag{3.2}$$

where λ_L and λ_R denote some characteristic wave velocities, and W_L^* and W_R^* are the intermediate states, to be detailed later. To ensure that $\lambda_L < 0$ and $\lambda_R > 0$, we choose the following expressions of λ_L and λ_R (see for instance [40] and references therein):

$$\lambda_L = \min\left(-|u_L| - c_L, -|u_R| - c_R, -\varepsilon_\lambda\right), \tag{3.3a}$$

$$\lambda_R = \max\left(|u_L| + c_L, |u_R| + c_R,\ \varepsilon_\lambda\right), \tag{3.3b}$$

with c the sound speed, defined by (1.4), and ε_λ a positive real value to be fixed in the numerical applications.

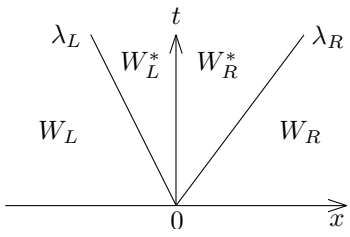

Figure 2: Structure of the chosen approximate Riemann solver.

The approximate solution of the Riemann problem $W^\Delta(x, t^n + t)$, depicted Figure 3, is given for $t > 0$ and $x \in (x_{i-\frac{1}{2}}, x_{i+\frac{1}{2}})$ by:

$$\forall i \in \mathbb{Z}, W^\Delta(x, t^n + t) = \begin{cases} W_{i-\frac{1}{2}}^{R,*} & \text{if } x \in [x_{i-\frac{1}{2}}, x_{i-\frac{1}{2}} + \lambda_{i-\frac{1}{2}}^R t], \\ W_i^n & \text{if } x \in [x_{i-\frac{1}{2}} + \lambda_{i-\frac{1}{2}}^R t, x_{i+\frac{1}{2}} + \lambda_{i+\frac{1}{2}}^L t], \\ W_{i+\frac{1}{2}}^{L,*} & \text{if } x \in [x_{i+\frac{1}{2}} + \lambda_{i+\frac{1}{2}}^L t, x_{i+\frac{1}{2}}]. \end{cases} \quad (3.4)$$

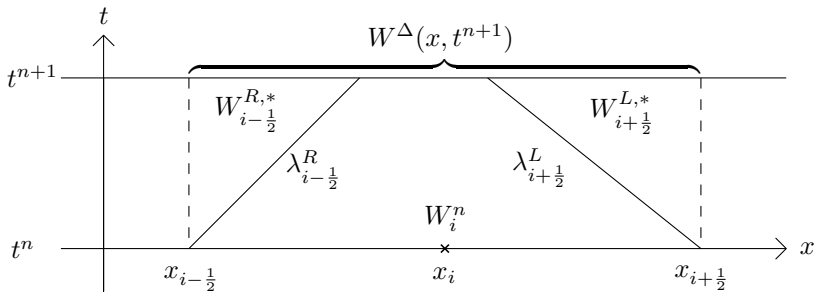

Figure 3: The full Godunov-type scheme using an approximate Riemann solver.

Now, we consider a time step Δt that satisfies the following Courant-Friedrichs-Lewy stability condition :

$$\Delta t \leq \frac{\Delta x}{2\Lambda}, \text{ where } \Lambda = \max_{i \in \mathbb{Z}} \left(\lambda_{i+\frac{1}{2}}^L, \lambda_{i+\frac{1}{2}}^R \right), \quad (3.5)$$

so as to ensure there are no interactions between the waves from two consecutive Riemann problems (see [20, 40]). Given such a Δt, we set $t^{n+1} = t^n + \Delta t$ and focus on the value of W^Δ at time t^{n+1}. We can finally define W_i^{n+1} by taking the average of $W^\Delta(x, t^{n+1})$ over the cell $(x_{i-\frac{1}{2}}, x_{i+\frac{1}{2}})$, as follows:

$$W_i^{n+1} = \frac{1}{\Delta x} \int_{x_{i-\frac{1}{2}}}^{x_{i+\frac{1}{2}}} W^\Delta(x, t^{n+1}) dx.$$

Since $W^{\Delta}(x, t^{n+1})$ is given by (3.4), we have:

$$W_i^{n+1} = \frac{1}{\Delta x}\int_{x_{i-\frac{1}{2}}}^{x_{i-\frac{1}{2}}+\lambda^R_{i-\frac{1}{2}}\Delta t} W^{R,*}_{i-\frac{1}{2}}dx + \frac{1}{\Delta x}\int_{x_{i+\frac{1}{2}}+\lambda^L_{i+\frac{1}{2}}\Delta t}^{x_{i+\frac{1}{2}}} W^{L,*}_{i+\frac{1}{2}}dx + \frac{1}{\Delta x}\int_{x_{i-\frac{1}{2}}+\lambda^R_{i-\frac{1}{2}}\Delta t}^{x_{i+\frac{1}{2}}+\lambda^L_{i+\frac{1}{2}}\Delta t} W_i^n dx.$$

This relation immediately yields:

$$W_i^{n+1} = W_i^n - \frac{\Delta t}{\Delta x}\left[\lambda^L_{i+\frac{1}{2}}\left(W^{L,*}_{i+\frac{1}{2}} - W_i^n\right) - \lambda^R_{i-\frac{1}{2}}\left(W^{R,*}_{i-\frac{1}{2}} - W_i^n\right)\right]. \tag{3.6}$$

Note that, in order for W_i^{n+1} to be fully defined, we only need to give explicit values to the intermediate states $W^{L,*}_{i+\frac{1}{2}}$ and $W^{R,*}_{i+\frac{1}{2}}$. The end of this section is devoted to finding suitable intermediate states, which ensure that the scheme is consistent and preserves the steady states.

3.2. A well-balanced approximate Riemann solver for the friction source term

We focus on the derivation of a well-balanced approximate Riemann solver for the shallow-water equations with only the friction source term. First, we recall the system under consideration:

$$\begin{cases} \partial_t h + \partial_x q &= 0, \\ \partial_t q + \partial_x\left(\dfrac{q^2}{h} + \dfrac{1}{2}gh^2\right) &= -kq|q|h^{-\eta}. \end{cases} \tag{3.7}$$

We also recall that the steady states for this model are given by:

$$\begin{cases} q = q_0, \\ \partial_x\left(\dfrac{q_0^2}{h} + \dfrac{1}{2}gh^2\right) = -kq|q|h^{-\eta}. \end{cases} \tag{3.8}$$

Relevant definitions of the intermediate states $W_L^* = {}^t(h_L^*, q_L^*)$ and $W_R^* = {}^t(h_R^*, q_R^*)$ need to be obtained in order to fully determine the approximate Riemann solver. Therefore, four equations characterizing the four unknowns h_L^*, h_R^*, q_L^* and q_R^* are required. These four equations will be obtained by considering two essential properties that need to be satisfied by the approximate Riemann solver: consistency with the system (3.7) and well-balancedness, i.e. preservation of the steady states (3.8).

First, we tackle the issue of the consistency with (3.7), by introducing a necessary consistency condition. From [25], the average over a cell of the approximate Riemann solver $\widetilde{W}$, defined by (3.2), has to be equal to the average over the same cell of the exact solution of the Riemann problem $W_{\mathcal{R}}$. Therefore, the following equality is imposed:

$$\frac{1}{\Delta x}\int_{-\Delta x/2}^{\Delta x/2}\widetilde{W}\left(\frac{x}{\Delta t}; W_L, W_R\right)dx = \frac{1}{\Delta x}\int_{-\Delta x/2}^{\Delta x/2} W_{\mathcal{R}}\left(\frac{x}{\Delta t}; W_L, W_R\right)dx. \tag{3.9}$$

We introduce the following notations for the sake of simplicity:

$$(\lambda_R - \lambda_L) h_{HLL} = \lambda_R h_R - \lambda_L h_L - [q],$$
$$(\lambda_R - \lambda_L) q_{HLL} = \lambda_R q_R - \lambda_L q_L - \left[\frac{q^2}{h} + \frac{1}{2} g h^2 \right].$$

Let us underline that ${}^t(h_{HLL}, q_{HLL})$ is actually the well-known intermediate state of the HLL approximate Riemann solver introduced in [25]. Also, note that $h_{HLL} > 0$ for λ_L and λ_R given by (3.3). We also introduce the notation $(-kq|q|h^{-\eta})_{\mathcal{R}}$ that denotes the second component of $s(W_{\mathcal{R}})$, with s defined by (1.3), to represent the value of the source term of friction for the exact solution of the Riemann problem. Thanks to these notations, (3.9) can be rewritten as follows, after straightforward computations detailed in [35]:

$$\lambda_R h_R^* - \lambda_L h_L^* = (\lambda_R - \lambda_L) h_{HLL}, \tag{3.10a}$$
$$\lambda_R q_R^* - \lambda_L q_L^* = (\lambda_R - \lambda_L) q_{HLL} + \frac{1}{\Delta t} \int_{-\Delta x/2}^{\Delta x/2} \int_0^{\Delta t} \left(-kq|q|h^{-\eta}\right)_{\mathcal{R}} \left(\frac{x}{t}; W_L, W_R\right) dt\, dx. \tag{3.10b}$$

Now, we introduce two parameters, $\bar{q}$ and $\overline{h^{-\eta}}$, to define a consistent approximation of the mean value of the friction source term, as follows:

$$\frac{1}{\Delta x} \frac{1}{\Delta t} \int_{-\Delta x/2}^{\Delta x/2} \int_0^{\Delta t} \left(-kq|q|h^{-\eta}\right)_{\mathcal{R}} dt\, dx \simeq -k\bar{q}|\bar{q}|\overline{h^{-\eta}}. \tag{3.11}$$

The parameters $\bar{q}$ and $\overline{h^{-\eta}}$ are respectively assumed to be consistent with q and $h^{-\eta}$, in a sense given later. Then, the equation (3.11) is substituted into (3.10b). As a consequence, the four unknowns are imposed to satisfy the following two relations:

$$\lambda_R h_R^* - \lambda_L h_L^* = (\lambda_R - \lambda_L) h_{HLL}, \tag{3.12a}$$
$$\lambda_R q_R^* - \lambda_L q_L^* = (\lambda_R - \lambda_L) q_{HLL} - k\bar{q}|\bar{q}|\overline{h^{-\eta}} \Delta x. \tag{3.12b}$$

Concerning the well-balancedness of the approximate Riemann solver, we exhibit a sufficient condition for the preservation of a solution. The scheme (3.6) provides us with such a condition. Indeed, the solution is obviously stationary, i.e. $W_i^{n+1} = W_i^n$ for all $i \in \mathbb{Z}$, if we have

$$\forall i \in \mathbb{Z}, \quad W_{i+\frac{1}{2}}^{L,*} = W_i^n \quad \text{and} \quad W_{i-\frac{1}{2}}^{R,*} = W_i^n.$$

Thus, in the context of the approximate Riemann solver, the solution will be stationary if $W_L^* = W_L$ and $W_R^* = W_R$. As a consequence, the following well-balance principle will have to be satisfied by the intermediate states:

Principle (WB). The intermediate states W_L^* and W_R^* are such that $W_L^* = W_L$ and $W_R^* = W_R$ as soon as W_L and W_R define a steady state.

Here, the pair (W_L, W_R) is said to define a steady state if they satisfy the identity (3.8). We will then look for intermediate states W_L^* and W_R^* that satisfy the (WB) principle.

We begin by determining q_L^* and q_R^*. After [4, 35], we choose $q_L^* = q_R^*$ and set $q^* := q_L^* = q_R^*$. This choice helps ensure that W_L^* and W_R^* satisfy the property (WB). The formulas (3.12) are then rewritten using q^* as follows:

$$\lambda_R h_R^* - \lambda_L h_L^* = (\lambda_R - \lambda_L) h_{HLL}, \tag{3.13a}$$

$$q^* = q_{HLL} - \frac{k\bar{q}|\bar{q}|\overline{h^{-\eta}}\Delta x}{\lambda_R - \lambda_L}. \tag{3.13b}$$

We only need relevant definitions of $\bar{q}$ and $\overline{h^{-\eta}}$ in order to fully determine q^*. To that end, we specify the discrete steady states verified by the system (3.7). Such discrete steady states are nothing but a discretization of the steady relation at the continuous level (3.8). In order to give an expression of these discrete steady states, we need to assume that $h_L \neq 0$ and $h_R \neq 0$. Now, W_L and W_R define a steady state if the following relations hold:

$$\begin{cases} q_L = q_R = q_0, & \text{(3.14a)} \\ q_0^2 \left[\dfrac{1}{h}\right] + \dfrac{g}{2}\left[h^2\right] = -k\bar{q}|\bar{q}|\overline{h^{-\eta}}\,\Delta x. & \text{(3.14b)} \end{cases}$$

Moreover, since we are only considering the friction source term and smooth steady states, we can rewrite the relation (2.3) between states W_L and W_R. Thus, W_L and W_R also satisfy the following algebraic relation:

$$-\frac{q_0^2}{\eta - 1}\left[h^{\eta-1}\right] + \frac{g}{\eta + 2}\left[h^{\eta+2}\right] = -kq_0|q_0|\,\Delta x. \tag{3.15}$$

We introduce the notation $\mu_0 = \operatorname{sgn}(q_0)$. Therefore, μ_0 represents the direction of the water flow. From (3.15), we obtain the evaluation of q_0^2 as follows:

$$q_0^2 = \frac{g\dfrac{[h^{\eta+2}]}{\eta+2}}{\dfrac{[h^{\eta-1}]}{\eta-1} - k\mu_0\,\Delta x}. \tag{3.16}$$

Now, to recover the behavior of the friction source term when steady states are involved, we assume that the parameter $\bar{q}$ is equal to q_0 as soon as W_L and W_R define a steady state. Thus, injecting (3.16) into (3.14b) yields the expression of $\overline{h^{-\eta}}$. We immediately obtain:

$$\overline{h^{-\eta}} = \frac{[h^2]}{2}\frac{\eta+2}{[h^{\eta+2}]} - \frac{\mu_0}{k\,\Delta x}\left(\left[\frac{1}{h}\right] + \frac{[h^2]}{2}\frac{[h^{\eta-1}]}{\eta-1}\frac{\eta+2}{[h^{\eta+2}]}\right). \tag{3.17}$$

Lemma 2. *The expression of $\overline{h^{-\eta}}$ given by (3.17) is consistent with $h^{-\eta}$.*

Proof. With smooth water heights, we fix, in (3.17), $h_L = h(x)$ and $h_R = h(x+\mathcal{O}(\Delta x))$. Taylor's formula applied to h_R yields $h_R = h+\Delta x\partial_x h+\mathcal{O}(\Delta x^2)$. In order to evaluate the Taylor expansions of $[h^2]$, $[h^{\eta-1}]$, $[h^{\eta+2}]$ and $[h^{-1}]$, we now compute a Taylor expansion, for some $\beta \in \mathbb{R}$, of the jump $[h^\beta]$:

$$\begin{aligned}[h^\beta] = h_R^\beta - h_L^\beta &= \left(h + \partial_x h\Delta x + \mathcal{O}(\Delta x^2)\right)^\beta - h^\beta \\ &= h^\beta\left(1 + \beta h^{-1}\partial_x h\Delta x + \mathcal{O}(\Delta x^2)\right) - h^\beta \\ &= \beta h^{\beta-1}\partial_x h\Delta x + \mathcal{O}(\Delta x^2).\end{aligned}$$

Using the above evaluation, we have for the first part of the expression of $\overline{h^{-\eta}}$:

$$\frac{[h^2]}{2}\frac{\eta+2}{[h^{\eta+2}]} = \frac{h\partial_x h\Delta x + \mathcal{O}(\Delta x^2)}{h^{\eta+1}\partial_x h\Delta x + \mathcal{O}(\Delta x^2)} = h^{-\eta} + \mathcal{O}(\Delta x). \tag{3.18}$$

Moreover, we have, for the second part of $\overline{h^{-\eta}}$,

$$\left[\frac{1}{h}\right] = -h^{-2}\partial_x h\Delta x + \mathcal{O}(\Delta x^2), \tag{3.19}$$

$$\begin{aligned}\frac{[h^2]}{2}\frac{[h^{\eta-1}]}{\eta-1}\frac{\eta+2}{[h^{\eta+2}]} &= \frac{(h\partial_x h\Delta x + \mathcal{O}(\Delta x^2))(h^{\eta-2}\partial_x h\Delta x + \mathcal{O}(\Delta x^2))}{h^{\eta+1}\partial_x h\Delta x + \mathcal{O}(\Delta x^2)} \\ &= h^{-2}\partial_x h\Delta x + \mathcal{O}(\Delta x^2).\end{aligned} \tag{3.20}$$

Combining both equations (3.19) and (3.20) immediately yields

$$-\frac{\mu_0}{k\,\Delta x}\left(\left[\frac{1}{h}\right] + \frac{[h^2]}{2}\frac{[h^{\eta-1}]}{\eta-1}\frac{\eta+2}{[h^{\eta+2}]}\right) = -\frac{\mu_0}{k\,\Delta x}\mathcal{O}(\Delta x^2) = \mathcal{O}(\Delta x). \tag{3.21}$$

Using both relations (3.18) and (3.21) gives $\overline{h^{-\eta}} = h^{-\eta} + \mathcal{O}(\Delta x)$, which concludes the proof. □

Concerning $\bar{q}$, we choose the following average:

$$\begin{cases}\bar{q} = \dfrac{2|q_L||q_R|}{|q_L|+|q_R|}\operatorname{sgn}(q_L+q_R) & \text{if } q_L \neq 0 \text{ and } q_R \neq 0; \\ \bar{q} = 0 & \text{if } q_L = 0, q_R = 0 \text{ or } k = 0.\end{cases} \tag{3.22}$$

This average indeed ensures that, if $q_L = q_R$, then $\bar{q} = q_L = q_R$.

Note that the expression (3.17) of $\overline{h^{-\eta}}$ contains μ_0. This quantity depends on the steady state and has to be determined for non-steady states. To address such an issue, we propose the expression

$$\overline{h^{-\eta}} := \overline{h^{-\eta}}(h_L, h_R) = \frac{[h^2]}{2}\frac{\eta+2}{[h^{\eta+2}]} - \frac{\bar{\mu}}{k\,\Delta x}\left(\left[\frac{1}{h}\right] + \frac{[h^2]}{2}\frac{[h^{\eta-1}]}{\eta-1}\frac{\eta+2}{[h^{\eta+2}]}\right), \tag{3.23}$$

where $\bar{\mu}$ is the sign of the quantity $\bar{q}$ given by (3.22). Since $\bar{q} = q_0$ as soon as W_L and W_R define a steady state, it is clear that $\overline{h^{-\eta}}$, as defined by (3.23),

still provides a well-balanced approximate Riemann solver and still satisfies Lemma 2.

Equipped with the expressions of $\overline{h^{-\eta}}$ and $\bar{q}$, we have fully determined q^*. Now, we need to complete the system (3.13) to determine the intermediate water heights h_L^* and h_R^*. The following relation is chosen to ensure that W_L^* and W_R^* satisfy the property (WB):

$$\alpha^f(h_R^* - h_L^*) = -k\bar{q}|\bar{q}|\overline{h^{-\eta}}\,\Delta x, \quad \text{where} \quad \alpha^f = \frac{-\bar{q}^2}{h_L h_R} + \frac{g}{2}(h_L + h_R). \tag{3.24}$$

Therefore, h_L^* and h_R^* are easily determined by considering the following linear system, defined by (3.13a) and (3.24):

$$\begin{cases} \lambda_R h_R^* - \lambda_L h_L^* = (\lambda_R - \lambda_L) h_{HLL}, \\ \alpha^f(h_R^* - h_L^*) = -k\bar{q}|\bar{q}|\overline{h^{-\eta}}\,\Delta x. \end{cases} \tag{3.25}$$

The system (3.25) is immediately solved, to get

$$h_L^* = h_{HLL} + \frac{\lambda_R k\bar{q}|\bar{q}|\overline{h^{-\eta}}\,\Delta x}{\alpha^f(\lambda_R - \lambda_L)}, \tag{3.26a}$$

$$h_R^* = h_{HLL} + \frac{\lambda_L k\bar{q}|\bar{q}|\overline{h^{-\eta}}\,\Delta x}{\alpha^f(\lambda_R - \lambda_L)}. \tag{3.26b}$$

3.3. Properties satisfied by the approximate Riemann solver

In the previous subsection, we have constructed intermediate states (3.13b) - (3.26) that yield a consistent and well-balanced approximate Riemann solver. However, one can plainly see from (3.26) that the intermediate water heights h_L^* and h_R^* can become negative. If that is the case, (3.6) can yield a negative updated water height, which means the updated state would not belong to the admissible space Ω. To recover this required robustness property, we apply the procedure from [2, 6, 35], which consists in introducing a parameter $\varepsilon > 0$, that controls the positivity of h_L^* and h_R^*.

We now state the expressions of the intermediate states obtained with this procedure, for given W_L and W_R. The parameter ε is such that

$$\varepsilon = \min\left(h_L,\, h_R,\, h_{HLL}\right). \tag{3.27}$$

For the sake of simplicity in the notations, we introduce the following notation:

$$\bar{S}^f := -k\bar{q}|\bar{q}|\overline{h^{-\eta}}, \tag{3.28}$$

where $\bar{q}$ and $\overline{h^{-\eta}}$ are respectively defined by (3.22) and (3.23). Then, the intermediate states $W_L^* = {}^t(h_L^*, q_L^*)$ and $W_R^* = {}^t(h_R^*, q_R^*)$ of the approximate Riemann

solver (3.2) are given by:

$$\alpha^f = \frac{-\bar{q}^2}{h_L h_R} + \frac{g}{2}(h_L + h_R), \tag{3.29a}$$

$$q_L^* = q_R^* = q^* = q_{HLL} + \frac{\overline{S}^f \Delta x}{\lambda_R - \lambda_L}, \tag{3.29b}$$

$$h_L^* = \min\left(\max\left(h_{HLL} - \frac{\lambda_R \overline{S}^f \, \Delta x}{\alpha^f(\lambda_R - \lambda_L)}, \varepsilon\right), \left(1 - \frac{\lambda_R}{\lambda_L}\right) h_{HLL} + \frac{\lambda_R}{\lambda_L}\varepsilon\right), \tag{3.29c}$$

$$h_R^* = \min\left(\max\left(h_{HLL} - \frac{\lambda_L \overline{S}^f \, \Delta x}{\alpha^f(\lambda_R - \lambda_L)}, \varepsilon\right), \left(1 - \frac{\lambda_L}{\lambda_R}\right) h_{HLL} + \frac{\lambda_L}{\lambda_R}\varepsilon\right). \tag{3.29d}$$

The quantities q^* and α^f have respectively been defined by (3.13b) and (3.24). Moreover, in (3.29), the positivity correction has been applied, and new expressions (3.29c) and (3.29d) of h_L^* and h_R^* have replaced (3.26a) and (3.26b). Note that the intermediate states (3.29) are written under the same form as the intermediate states presented in [35].

The following two results sum up the properties we have obtained thus far, for the approximate Riemann solver and the full scheme. For the sake of conciseness, we do not mention their proofs here, since they use classical ingredients that have been presented in [35].

Lemma 3. *Assume $\varepsilon > 0$ such that (3.27) is satisfied. Then, intermediate states $W_L^* = {}^t(h_L^*, q_L^*)$ and $W_R^* = {}^t(h_R^*, q_R^*)$ given by (3.29) satisfy the following properties:*

(i) consistency: the quantities h_L^*, h_R^*, q_L^* and q_R^* satisfy the equations (3.13);

(ii) positivity preservation: if $h_L > 0$, $h_R > 0$ and $h_{HLL} > 0$, then $h_L^* \geq \varepsilon$ and $h_R^* \geq \varepsilon$;

(iii) well-balancedness: $W_L^* = W_L$ and $W_R^* = W_R$ satisfy the property (WB).

Theorem 4. *Consider $W_i^n \in \Omega^*$ for all $i \in \mathbb{Z}$, where Ω^* is a restricted admissible states space defined as follows:*

$$\Omega^* = \left\{ W = {}^t(h, q) \in \mathbb{R}^2 \ ; \ h > 0, \, q \in \mathbb{R} \right\}.$$

Assume that the intermediate states $W_{i+\frac{1}{2}}^{L,*}$ and $W_{i+\frac{1}{2}}^{R,*}$ are given, for all $i \in \mathbb{Z}$, by

$$W_{i+\frac{1}{2}}^{L,*} = \begin{pmatrix} h_L^*(W_i^n, W_{i+1}^n) \\ q^*(W_i^n, W_{i+1}^n) \end{pmatrix} \quad \text{and} \quad W_{i+\frac{1}{2}}^{R,*} = \begin{pmatrix} h_R^*(W_i^n, W_{i+1}^n) \\ q^*(W_i^n, W_{i+1}^n) \end{pmatrix},$$

where q^*, h_L^* and h_R^* are given by (3.29b), (3.29c) and (3.29d), respectively. Also, assume $\varepsilon > 0$ given by (3.27). Then the Godunov-type scheme, given by (3.6) under the CFL restriction (3.5), satisfies the following properties:

1. *consistency with the shallow-water system* (3.7)*;*
2. *positivity preservation:* $\forall i \in \mathbb{Z}$, $W_i^{n+1} \in \Omega^*$*;*
3. *well-balancedness: if* $(W_i^n)_{i\in\mathbb{Z}}$ *defines a steady state, then* $\forall i \in \mathbb{Z}$, $W_i^{n+1} = W_i^n$.

From the above result, we see that the updated water height never vanishes. This behavior is due to the introduction in (3.29) of the parameter ε. Such a behavior is necessary because the average $\overline{h^{-\eta}}$ has been obtained by considering positive water heights. In a later section, devoted to dry/wet transitions, this average will be extended to be able to deal with dry areas. This extension will allow us to consider $\varepsilon = 0$ in the definition (3.29), as well as vanishing water heights.

4. The case of both topography and friction source terms

In this section, our goal is the derivation of new intermediate states h_L^*, h_R^* and q^* to approximate the contributions of both topography and friction source terms. For the sake of simplicity in the notations, we write $S = S^t + S^f$, where

$$\begin{aligned} S^t &= -gh\partial_x Z, \\ S^f &= -kq|q|h^{-\eta}, \end{aligned}$$

which corresponds to the case where both topography and friction source terms are involved. The steady states associated to the full source term S do not admit an algebraic expression. Therefore S is split between S^t and S^f, since the steady states for the individual source terms of topography and friction can both be rewritten using an algebraic expression. In order to complete the scheme, we need to determine suitable intermediate states in both cases of the topography and the friction. The case of the friction has been treated in the previous section, and the intermediate states are given by (3.29). For the topography, we adopt the approach introduced in [35], which is now recalled for the sake of completeness.

4.1. Approximation of the topography source term

Considering a vanishing topography source term but with a vanishing friction, the intermediate states are given by

$$\alpha^t = \frac{-(q^*)^2}{h_L h_R} + \frac{g}{2}(h_L + h_R), \tag{4.1a}$$

$$q_L^* = q_R^* = q^* = q_{HLL} + \frac{\overline{S}^t \Delta x}{\lambda_R - \lambda_L}, \tag{4.1b}$$

$$h_L^* = \min\left(\max\left(h_{HLL} - \frac{\lambda_R \overline{S}^t \Delta x}{\alpha^t(\lambda_R - \lambda_L)}, \varepsilon\right), \left(1 - \frac{\lambda_R}{\lambda_L}\right) h_{HLL} + \frac{\lambda_R}{\lambda_L}\varepsilon\right), \tag{4.1c}$$

$$h_R^* = \min\left(\max\left(h_{HLL} - \frac{\lambda_L \overline{S}^t \Delta x}{\alpha^t(\lambda_R - \lambda_L)}, \varepsilon\right), \left(1 - \frac{\lambda_L}{\lambda_R}\right) h_{HLL} + \frac{\lambda_L}{\lambda_R}\varepsilon\right). \tag{4.1d}$$

In (4.1), the approximate topography source term $\overline{S}^t$ is defined by:

$$\overline{S}^t \Delta x := \overline{S}^t(h_L, h_R, Z_L, Z_R)\Delta x = -2g[Z]\frac{h_L h_R}{h_L + h_R} + \frac{g}{2}\frac{[h]_c^3}{h_L + h_R}, \tag{4.2}$$

where $[h]_c$ is a cutoff of $[h] = h_R - h_L$, defined as follows:

$$[h]_c = \begin{cases} h_R - h_L & \text{if } |h_R - h_L| \leq C\,\Delta x, \\ \operatorname{sgn}(h_R - h_L) C\,\Delta x & \text{otherwise,} \end{cases} \tag{4.3}$$

with C a positive constant that does not depend on Δx. This expression of $\overline{S}^t$ is consistent with the topography source term S^t, and it ensures that the scheme is well-balanced (see [4, 5, 35] for more details regarding this expression and how to obtain it). Computations leading to this expression and to the expressions (4.1) have been explained in [35], to which the reader is referred for more details.

4.2. Approximation of the topography and friction source terms

Now, we focus on deriving intermediate states for the shallow-water equations with both topography and friction source terms. We introduce the following discretization of (1.7):

$$q_0^2 \left[\frac{1}{h}\right] + \frac{g}{2}\left[h^2\right] = \overline{S}^t \Delta x + \overline{S}^f \Delta x, \tag{4.4}$$

where the approximate source term $\overline{S}$ has been split into the topography and friction contributions, by writing $\overline{S} = \overline{S}^t + \overline{S}^f$. As a consequence, after (3.29b), we define the following intermediate discharge:

$$q^* = q_{HLL} + \frac{\overline{S}^t \Delta x}{\lambda_R - \lambda_L} + \frac{\overline{S}^f \Delta x}{\lambda_R - \lambda_L}, \tag{4.5}$$

where the expressions of $\overline{S}^t$ and $\overline{S}^f$ are given by (4.2) and (3.28), respectively. Concerning the intermediate heights, we first decide to use the following expressions:

$$\widetilde{h_L^*} = h_{HLL} - \frac{\lambda_R \overline{S}^t \Delta x}{\alpha^t(\lambda_R - \lambda_L)} - \frac{\lambda_R \overline{S}^f \Delta x}{\alpha^f(\lambda_R - \lambda_L)}, \tag{4.6a}$$

$$\widetilde{h_R^*} = h_{HLL} - \frac{\lambda_L \overline{S}^t \Delta x}{\alpha^t(\lambda_R - \lambda_L)} - \frac{\lambda_L \overline{S}^f \Delta x}{\alpha^f(\lambda_R - \lambda_L)}, \tag{4.6b}$$

where the quantities α^t and α^f are respectively defined by (4.1a) and (3.29a). We immediately see that the intermediate states (4.5) - (4.6) still yield a consistent scheme. Moreover, it is possible to recover the positivity of the water heights. Let $\varepsilon \geq 0$ that satisfies (3.27), and consider the same procedure as used for the friction source term, which yields the following intermediate states:

$$q^* = q_{HLL} + \frac{\overline{S}^t \Delta x}{\lambda_R - \lambda_L} + \frac{\overline{S}^f \Delta x}{\lambda_R - \lambda_L}, \tag{4.7a}$$

$$h_L^* = \min\left(\max\left(\widetilde{h_L^*}, \varepsilon\right), \left(1 - \frac{\lambda_R}{\lambda_L}\right) h_{HLL} + \frac{\lambda_R}{\lambda_L}\varepsilon\right), \tag{4.7b}$$

$$h_R^* = \min\left(\max\left(\widetilde{h_R^*}, \varepsilon\right), \left(1 - \frac{\lambda_L}{\lambda_R}\right) h_{HLL} + \frac{\lambda_L}{\lambda_R}\varepsilon\right). \tag{4.7c}$$

From Lemma 3, as soon as $\varepsilon > 0$, the intermediate heights h_L^* and h_R^* defined by (4.7) are positive.

We note that using the definitions (4.7) and making the friction source term vanish allows the recovery of the intermediate states for topography only. Similarly, if the topography source term vanishes, we recover the intermediate states for friction only. As a consequence, (4.7) yields intermediate states that are well-balanced for the individual source terms of topography or friction.

Let us recall that the steady states relation for the shallow-water system with both topography and friction source terms (1.5) cannot be written under the form of an algebraic relation for all Z. Therefore, we only manage to preserve the steady states up to the chosen discretization (4.4) of (1.7) (see [16, 28, 33, 46, 47] where a similar approach is used).

We finally study how the approximate source term averages $\overline{S}^t$ and $\overline{S}^f$, as well as the terms $\overline{S}^t \Delta x/\alpha^t$ and $\overline{S}^f \Delta x/\alpha^f$, behave when dealing with vanishing water heights. First, we make the following assumption.

Assumption. When the height vanishes, so does the velocity.

This assumption allows us to state the following result, concerning the approximate topography source term.

Lemma 5. *When h_L or h_R vanishes, the quantities $\overline{S}^t$ and $\overline{S}^t \Delta x/\alpha^t$ satisfy:*

$$\overline{S}^t \Delta x = -g\,(Z_R - Z_L)\,\frac{h_R + h_L}{2} \quad \textit{and} \quad \frac{\overline{S}^t \Delta x}{\alpha^t} = -\,(Z_R - Z_L)\,.$$

The reader is referred to [35] for the detailed proof of this result. We then turn to the approximate friction source term. We have to make the following assumption in order to define it for vanishing water heights.

Assumption. Using $\overline{S}^f$ and α^f respectively defined by (3.28) and (3.29a), we impose that $\overline{S}^f$ and $\overline{S}^f/\alpha^f$ are zero as soon as h_L and/or h_R vanishes.

It makes sense to consider such a behavior. Indeed, as previously mentioned, the friction contribution is assumed to vanish as soon as the water height vanishes. In order for both quantities $\overline{S}^f$ and $\overline{S}^f/\alpha^f$ to satisfy this requirement, we have to impose that they vanish when h_L and/or h_R vanishes.

To handle the case where both h_L and h_R vanish (and thus $q_L = q_R = 0$), we have to make sure that, in this case, $q^* = 0$ and $h_L^* = h_R^* = 0$. This requirement is met by taking $\overline{S}^t = 0$ and $\overline{S}^t/\alpha^t = 0$, as well as $\overline{S}^f = 0$ and $\overline{S}^f/\alpha^f = 0$, as soon as both h_L and h_R are zero.

We can now state the following result, concerning the approximate Riemann solver for both source terms of topography and friction.

Lemma 6. *The intermediate states (4.7) satisfy the following properties:*

(i) consistency with the shallow-water equations with topography and friction (1.1);

(ii) well-balancedness: if W_L and W_R define a steady state, i.e. satisfy (4.4), then $W_L^* = W_L$ and $W_R^* = W_R$.

Moreover, we have:

(iii) with $\varepsilon > 0$, the positivity is preserved: if $h_L > 0$, $h_R > 0$ and $h_{HLL} > 0$, then $h_L^* \geq \varepsilon$ and $h_R^* \geq \varepsilon$;

(iv) with $\varepsilon = 0$, the non-negativity is preserved: if $h_L \geq 0$, $h_R \geq 0$ and $h_{HLL} \geq 0$, then $h_L^* \geq 0$ and $h_R^* \geq 0$.

Proof. For $\varepsilon > 0$, the proofs of (i), (ii) and (iii) are immediate. They come from Lemma 3 as well as the results obtained in the current section. Now, assume $\varepsilon = 0$. The intermediate states then rewrite:

$$q^* = q_{HLL} + \frac{\overline{S}^t \Delta x}{\lambda_R - \lambda_L} + \frac{\overline{S}^f \Delta x}{\lambda_R - \lambda_L}, \tag{4.8a}$$

$$h_L^* = \min\left(\left(h_{HLL} - \frac{\lambda_R \overline{S}^t \Delta x}{\alpha^t(\lambda_R - \lambda_L)} - \frac{\lambda_R \overline{S}^f \Delta x}{\alpha^f(\lambda_R - \lambda_L)}\right)_+, \left(1 - \frac{\lambda_R}{\lambda_L}\right) h_{HLL}\right), \tag{4.8b}$$

$$h_R^* = \min\left(\left(h_{HLL} - \frac{\lambda_L \overline{S}^t \Delta x}{\alpha^t(\lambda_R - \lambda_L)} - \frac{\lambda_L \overline{S}^f \Delta x}{\alpha^f(\lambda_R - \lambda_L)}\right)_+, \left(1 - \frac{\lambda_L}{\lambda_R}\right) h_{HLL}\right). \tag{4.8c}$$

From the computations on the limits of the approximate source terms when h_L and h_R tend to 0 and by definition of $\overline{S}^t$ and $\overline{S}^f$, the above expressions are well-defined for all $h_L \geq 0$ and $h_R \geq 0$. Moreover, these new intermediate states can be easily shown (see the proof of Lemma 3) to satisfy properties (i), (ii) and (iv). Indeed, the proof of the consistency stated Lemma 3 is preserved, and thus (i) holds. Then, (iv) is a direct consequence of the fact that h_L^* and h_R^* are defined as the minimum of non-negative quantities.

Finally, concerning (ii) with $\varepsilon = 0$, we assume that W_L and W_R define a steady state according to (4.4). If $h_L > 0$, $h_R > 0$ and $h_{HLL} > 0$, then we know from Lemma 3 that $W_L^* = W_L$ and $W_R^* = W_R$. To handle the case where h_L or h_R is zero, we first note that we still have $q^* = q_0$. To conclude the proof of (ii), we have to show $h_L^* = h_L$ and $h_R^* = h_R$ if $h_L = 0$ or $h_R = 0$. For the sake of simplicity, we assume that $h_L = 0$. Then, $u_L = 0$, and $q_0 = 0$. From (4.4), we get:

$$\frac{g}{2}\left[h^2\right] = \overline{S}^t \Delta x + \overline{S}^f \Delta x, \tag{4.9}$$

Now, recall that the friction source term vanishes when $q_0 = 0$. From the expression (3.28) of $\overline{S}^f$, this approximate friction source term also vanishes as soon as $q_0 = 0$. Thus, using Lemma 5, the equation (4.9) rewrites after straightforward computations

$$h_R = -Z_R + Z_L.$$

We can now compute h_L^* and h_R^*. First, consider the expressions (4.6). In this case, they rewrite

$$\widetilde{h_L^*} = h_{HLL} - \frac{\lambda_R \left(Z_R - Z_L\right)}{\lambda_R - \lambda_L} = \frac{\lambda_R h_R - \lambda_R h_R}{\lambda_R - \lambda_L} = 0,$$
$$\widetilde{h_R^*} = h_{HLL} - \frac{\lambda_L \left(Z_R - Z_L\right)}{\lambda_R - \lambda_L} = \frac{\lambda_R h_R - \lambda_L h_R}{\lambda_R - \lambda_L} = h_R.$$

Thus, (4.8b) and (4.8c) immediately yield $h_L^* = h_L = 0$ and $h_R^* = h_R$. Similar computations show that we have the same result if h_R vanishes instead of h_L. Finally, if both h_L and h_R vanish, then h_{HLL} also vanishes, and we obtain $h_L^* = 0$ and $h_R^* = 0$. Thus, the proof is achieved. □

This lemma allows us to state the following result, that concerns the full scheme (3.6).

Theorem 7. *Consider $W_i^n \in \Omega$ for all $i \in \mathbb{Z}$. Assume that the intermediate states $W_{i+\frac{1}{2}}^{L,*}$ and $W_{i+\frac{1}{2}}^{R,*}$ are given, for all $i \in \mathbb{Z}$, by*

$$W_{i+\frac{1}{2}}^{L,*} = \begin{pmatrix} h_L^*(W_i^n, W_{i+1}^n) \\ q^*(W_i^n, W_{i+1}^n) \end{pmatrix} \quad \text{and} \quad W_{i+\frac{1}{2}}^{R,*} = \begin{pmatrix} h_R^*(W_i^n, W_{i+1}^n) \\ q^*(W_i^n, W_{i+1}^n) \end{pmatrix}, \tag{4.10}$$

where q^*, h_L^* and h_R^* are given by (4.8). Then the Godunov-type scheme, given by (3.6) under the CFL restriction (3.5), satisfies the following properties:

1. *consistency with the shallow-water system* (1.1);

2. *non-negativity preservation:* $\forall i \in \mathbb{Z}$, $W_i^{n+1} \in \Omega$;

3. *well-balancedness: if* $(W_i^n)_{i\in\mathbb{Z}}$ *defines a steady state according to* (4.4), *then* $\forall i \in \mathbb{Z}$, $W_i^{n+1} = W_i^n$. *The same result holds for both topography-only and friction-only steady states, respectively given by* (1.9) *and* (1.10).

Proof. The same arguments as used in the proof of Theorem 4, while using the results of Lemma 6, yield the proof of the theorem. □

5. Implicitation of the source terms contribution: wet/dry transitions

The scheme (3.6) - (4.10) allows the simulation of wet/dry transitions. However, several spurious oscillations appear when such experiments are performed. The stiffness of the source terms in the vicinity of wet/dry transitions, especially the friction, induces these spurious oscillations. To correct such a failure, we first rewrite this scheme in order to exhibit the numerical flux function and the source terms contribution. Then, we adopt an explicit scheme for the transport part, and an implicit scheme for the source part.

5.1. Reformulation of the scheme

In this subsection, we exhibit the numerical flux function and the numerical source terms. To that end, the scheme (3.6), with intermediate states given by (4.7), is rewritten after straightforward computations as follows (see for instance [25]):

$$W_i^{n+1} = W_i^n - \frac{\Delta t}{\Delta x}\left(f_{i+\frac{1}{2}}^n - f_{i-\frac{1}{2}}^n\right) + \frac{\Delta t}{2}\left(s_{i+\frac{1}{2}}^n + s_{i-\frac{1}{2}}^n\right). \tag{5.1}$$

The quantity $f_{i+\frac{1}{2}}^n = f(W_i^n, W_{i+1}^n)$ is the numerical flux function evaluated at the interface $x_{i+\frac{1}{2}}$, and the quantity $s_{i+\frac{1}{2}}^n$ is the numerical source term at the interface $x_{i+\frac{1}{2}}$. These quantities are approximations of the flux and the source term, respectively, and are defined by:

$$f_{i+\frac{1}{2}}^n = \begin{pmatrix} (f^h)_{i+\frac{1}{2}}^n \\ (f^q)_{i+\frac{1}{2}}^n \end{pmatrix} \quad \text{and} \quad s_{i+\frac{1}{2}}^n = \begin{pmatrix} 0 \\ (S^t)_{i+\frac{1}{2}}^n + (S^f)_{i+\frac{1}{2}}^n \end{pmatrix}. \tag{5.2}$$

The quantities $(S^t)_{i+\frac{1}{2}}^n$ and $(S^f)_{i+\frac{1}{2}}^n$ are approximations of the topography and the friction source terms, respectively. Adopting extended notations, they are given by:

$$(S^t)_{i+\frac{1}{2}}^n = \overline{S}^t\left(h_i^n, h_{i+1}^n, Z_i, Z_{i+1}\right), \tag{5.3a}$$

$$(S^f)_{i+\frac{1}{2}}^n = \overline{S}^f\left(h_i^n, h_{i+1}^n, q_i^n, q_{i+1}^n\right), \tag{5.3b}$$

where $\overline{S}^t$ and $\overline{S}^f$ are the approximate source terms already defined by (4.2) and (3.28). The scheme (5.1) then reads:

$$h_i^{n+1} = h_i^n - \frac{\Delta t}{\Delta x}\left((f^h)_{i+\frac{1}{2}}^n - (f^h)_{i-\frac{1}{2}}^n\right), \tag{5.4a}$$

$$\begin{aligned} q_i^{n+1} = q_i^n &- \frac{\Delta t}{\Delta x}\left((f^q)_{i+\frac{1}{2}}^n - (f^q)_{i-\frac{1}{2}}^n\right) \\ &+ \frac{\Delta t}{2}\left((S^t)_{i+\frac{1}{2}}^n + (S^t)_{i-\frac{1}{2}}^n + (S^f)_{i+\frac{1}{2}}^n + (S^f)_{i-\frac{1}{2}}^n\right), \end{aligned} \tag{5.4b}$$

where the approximate fluxes are defined by (5.2) and

$$\begin{aligned} f_{i+\frac{1}{2}}^n = &\frac{1}{2}\left(F(W_i^n) + F(W_{i+1}^n)\right) \\ &+ \frac{\lambda_{i+\frac{1}{2}}^L}{2}\left(W_{i+\frac{1}{2}}^{L,*} - W_i^n\right) + \frac{\lambda_{i+\frac{1}{2}}^R}{2}\left(W_{i+\frac{1}{2}}^{R,*} - W_{i+1}^n\right). \end{aligned} \tag{5.5}$$

For the sake of simplicity, we set:

$$(S^t)_i^n = \frac{1}{2}\left((S^t)_{i-\frac{1}{2}}^n + (S^t)_{i+\frac{1}{2}}^n\right) \quad \text{and} \quad (S^f)_i^n = \frac{1}{2}\left((S^f)_{i-\frac{1}{2}}^n + (S^f)_{i+\frac{1}{2}}^n\right), \tag{5.6}$$

such that (5.4b) rewrites:

$$q_i^{n+1} = q_i^n - \frac{\Delta t}{\Delta x}\left((f^q)_{i+\frac{1}{2}}^n - (f^q)_{i-\frac{1}{2}}^n\right) + \Delta t (S^t)_i^n + \Delta t (S^f)_i^n. \tag{5.7}$$

5.2. Implicitation of the source terms contribution

We now introduce a semi-implicit version of the Godunov-type scheme (5.1). The main idea of this section is to use a splitting method (see for instance [10, 40]) to reduce the impact of the aforementioned instabilities. The splitting strategy we use here is to first consider an explicit treatment of the flux, then an implicit treatment of both source terms. As a consequence, the first step, devoted to the transport part $\partial_t W + \partial_x f(W) = 0$, reads as follows:

$$h_i^{n+\frac{1}{3}} = h_i^n - \frac{\Delta t}{\Delta x}\left((f^h)_{i+\frac{1}{2}}^n - (f^h)_{i-\frac{1}{2}}^n\right), \tag{5.8a}$$

$$q_i^{n+\frac{1}{3}} = q_i^n - \frac{\Delta t}{\Delta x}\left((f^q)_{i+\frac{1}{2}}^n - (f^q)_{i-\frac{1}{2}}^n\right). \tag{5.8b}$$

During the second step, devoted to the topography source term, we approximately solve the initial value problem

$$\begin{cases} \dfrac{dh}{dt} = 0, \\ \dfrac{dq}{dt} = S^t(W), \end{cases} \quad \text{with initial data} \quad \begin{cases} h(0) = h_i^{n+\frac{1}{3}}, \\ q(0) = q_i^{n+\frac{1}{3}}, \end{cases}$$

where $S^t(W) = -gh\partial_t Z$. We suggest the following implicit scheme to approximate $h_i^{n+\frac{2}{3}}$ and $q_i^{n+\frac{2}{3}}$:

$$\begin{cases} h_i^{n+\frac{2}{3}} = h_i^{n+\frac{1}{3}}, & \text{(5.9a)} \\ q_i^{n+\frac{2}{3}} = q_i^{n+\frac{1}{3}} + \Delta t (S^t)_i^{n+\frac{2}{3}}, & \text{(5.9b)} \end{cases}$$

where, as per (5.6), $(S^t)_i^{n+\frac{2}{3}} = \left((S^t)_{i+\frac{1}{2}}^{n+\frac{2}{3}} + (S^t)_{i-\frac{1}{2}}^{n+\frac{2}{3}} \right)/2$, with, after (5.3a),

$$(S^t)_{i+\frac{1}{2}}^{n+\frac{2}{3}} = \bar{S}^t \left(h_i^{n+\frac{2}{3}}, h_{i+1}^{n+\frac{2}{3}}, Z_i, Z_{i+1} \right).$$

Let us underline that, during the second step, the evaluation of the implicit unknowns is immediate since the topography source term involves known quantities.

The third and last step concerns the friction and consists in solving

$$\begin{cases} \dfrac{dh}{dt} = 0, \\ \dfrac{dq}{dt} = -kq|q|(h_i^{n+1})^{-\eta}, \end{cases} \quad \text{with initial data} \quad \begin{cases} h(0) = h_i^{n+\frac{2}{3}}, \\ q(0) = q_i^{n+\frac{2}{3}}. \end{cases} \tag{5.10}$$

This system can be solved to find an analytic expression of the solution. For $t \in [0, \Delta t]$, the exact solution of the above system reads as follows:

$$\begin{cases} h(t) = h(0), & \text{(5.11a)} \\ q(t) = \dfrac{h(0)^\eta q(0)}{h(0)^\eta + k\, t\, |q(0)|}. & \text{(5.11b)} \end{cases}$$

Note that the analytic expression (5.11) guarantees that, for all $t \in (0, \Delta t]$, the sign of $q(t)$ stays the same as the sign of $q(0)$, and that $|q(t)| < |q(0)|$. This behavior is consistent with the fact that friction should only slow the movement of the fluid down, rather than changing its direction. Then, evaluating (5.11) at $t = \Delta t$ and plugging the initial data yields

$$\begin{cases} h_i^{n+1} = h_i^{n+\frac{2}{3}}, & \text{(5.12a)} \\ q_i^{n+1} = \dfrac{\left(h_i^{n+1}\right)^\eta q_i^{n+\frac{2}{3}}}{\left(h_i^{n+1}\right)^\eta + k\, \Delta t\, |q_i^{n+\frac{2}{3}}|}. & \text{(5.12b)} \end{cases}$$

Let us note that the updated state ${}^t(h_i^{n+1}, q_i^{n+1})$ retains its non-negativity preservation property, since the computations for h_i^{n+1} have not been modified and Theorem 7 applies. Furthermore, the expression (5.12b) is well-posed for $h_i^{n+1} = 0$ and, when that is the case, forces the discharge q_i^{n+1} to vanish. However, the well-balance property is lost. Indeed, if W_{i-1}^n, W_i^n and W_{i+1}^n define a steady state, we do not necessarily recover $q_i^{n+1} = q_i^n$. As a consequence, we decide to consider an approximation of $\left(h_i^{n+1}\right)^\eta$, denoted by $(\overline{h^\eta})_i^{n+1}$, in

(5.12b). This approximation is determined in order to ensure the required well-balancedness of the scheme.

In order to obtain such an expression of $(\overline{h^\eta})_i^{n+1}$, we momentarily suppose that W_{i-1}^n, W_i^n and W_{i+1}^n define a steady state. In this case, we need to ensure that $W_i^{n+1} = W_i^n$. Since the scheme (5.1) is well-balanced, the equation (5.7) yields $q_i^{n+1} = q_i^n$, and can be rewritten as:

$$(S^f)_i^n = \frac{1}{\Delta x}\left((f^q)_{i+\frac{1}{2}}^n - (f^q)_{i-\frac{1}{2}}^n\right) - (S^t)_i^n. \tag{5.13}$$

Moreover, we have $h_i^{n+\frac{2}{3}} = h_i^n$. Therefore, by the definition (5.3a) of $(S^t)_i^n$, we have $(S^t)_i^{n+\frac{2}{3}} = (S^t)_i^n$. The evaluation of $q_i^{n+\frac{2}{3}}$ is then obtained from (5.9b) as follows:

$$q_i^{n+\frac{2}{3}} = q_i^n - \frac{\Delta t}{\Delta x}\left((f^q)_{i+\frac{1}{2}}^n - (f^q)_{i-\frac{1}{2}}^n\right) + \Delta t (S^t)_i^n. \tag{5.14}$$

From (5.13) and (5.14), we immediately obtain

$$q_i^{n+\frac{2}{3}} = q_i^n - \Delta t (S^f)_i^n.$$

Thus, when steady states are assumed and using $(\overline{h^\eta})_i^{n+1}$, (5.12b) reads

$$q_i^n = \frac{(\overline{h^\eta})_i^{n+1}\left(q_i^n - \Delta t (S^f)_i^n\right)}{(\overline{h^\eta})_i^{n+1} + k\,\Delta t\,\left|q_i^n - \Delta t (S^f)_i^n\right|}. \tag{5.15}$$

We are now able to determine the expression of $(\overline{h^\eta})_i^{n+1}$ that ensures the well-balancedness of the scheme. We set $\mu_i^n = \operatorname{sgn} q_i^n$ and $\mu_i^{n+\frac{2}{3}} = \operatorname{sgn} q_i^{n+\frac{2}{3}}$. In order to simplify the expression of the scheme, we propose to introduce a new definition of $(S^f)_i^n$ to be substituted in (5.6). We suggest the following formula:

$$(S^f)_i^n = \frac{1}{2}\left(-k q_i^n |q_i^n| \left(\overline{h^{-\eta}}\right)_{i-\frac{1}{2}}^{n+1} - k q_i^n |q_i^n| \left(\overline{h^{-\eta}}\right)_{i+\frac{1}{2}}^{n+1}\right), \tag{5.16}$$

where $(\overline{h^{-\eta}})_{i-\frac{1}{2}}^{n+1}$ and $(\overline{h^{-\eta}})_{i+\frac{1}{2}}^{n+1}$ are given with clear notations by (3.23). In addition, for the sake of consistency, we have chosen to substitute $(\overline{\mu})_{i-\frac{1}{2}}^n$ and $(\overline{\mu})_{i+\frac{1}{2}}^n$ with μ_i^n. With this simplification in the source term approximation, we get the following expression for $(\overline{h^\eta})_i^{n+1}$, from (5.15) and (5.16):

$$(\overline{h^\eta})_i^{n+1} = \frac{2\mu_i^{n+\frac{2}{3}}\mu_i^n}{\left(\overline{h^{-\eta}}\right)_{i-\frac{1}{2}}^{n+1} + \left(\overline{h^{-\eta}}\right)_{i+\frac{1}{2}}^{n+1}} + k\,\Delta t\,\mu_i^{n+\frac{2}{3}} q_i^n.$$

The above expression can then be rewritten as

$$(\overline{h^\eta})_i^{n+1} = \frac{2k\mu_i^{n+\frac{2}{3}}\Delta x}{k\mu_i^n \Delta x\left(\beta_{i-\frac{1}{2}}^{n+1} + \beta_{i+\frac{1}{2}}^{n+1}\right) - \left(\gamma_{i-\frac{1}{2}}^{n+1} + \gamma_{i+\frac{1}{2}}^{n+1}\right)} + k\,\Delta t\,\mu_i^{n+\frac{2}{3}} q_i^n, \tag{5.17}$$

where we have set

$$\beta_{i+\frac{1}{2}}^{n+1} = \frac{\eta+2}{2} \frac{\left(h_{i+1}^{n+1}\right)^2 - \left(h_i^{n+1}\right)^2}{\left(h_{i+1}^{n+1}\right)^{\eta+2} - \left(h_i^{n+1}\right)^{\eta+2}} \text{ , and}$$

$$\gamma_{i+\frac{1}{2}}^{n+1} = \frac{1}{h_{i+1}^{n+1}} - \frac{1}{h_i^{n+1}} + \beta_{i+\frac{1}{2}}^{n+1} \frac{\left(h_{i+1}^{n+1}\right)^{\eta-1} - \left(h_i^{n+1}\right)^{\eta-1}}{\eta-1}.$$

Computations within the expression of $(\overline{h^\eta})_i^{n+1}$ show that it tends to 0 as soon as h_{i-1}^{n+1}, h_i^{n+1} or h_{i+1}^{n+1} tends to 0, which is a good behavior when dealing with wet/dry transitions. We have therefore devised a way to consider the source terms contribution in an implicit way, while still retaining the well-balance property of the scheme. We can thus state the following result.

Theorem 8. *The scheme* (5.8) - (5.9) - (5.12) - (5.17) *is positivity-preserving and well-balanced. Indeed, if* $(W_i^n)_{i\in\mathbb{Z}}$ *defines a steady state according to* (4.4)*, then* $\forall i \in \mathbb{Z}$, $W_i^{n+1} = W_i^n$. *The same result holds for both topography-only and friction-only steady states, respectively given by* (1.9) *and* (1.10).

Proof. We begin this proof by recalling that, from (5.8), (5.9) and (5.12), we have $h_i^{n+1} = h_i^{n+\frac{1}{3}}$. Therefore, since $h_i^{n+\frac{1}{3}}$ is given by the full scheme (3.6), which is positivity-preserving, the scheme under consideration is positivity-preserving. We now have to show that it is well-balanced. To that end, assume that W_{i-1}^n, W_i^n and W_{i+1}^n define a steady state, according to (4.4), (1.9) or (1.10). Using a similar chain of arguments as above, we immediately recover that $h_i^{n+1} = h_i^n$. To complete the proof, we now have to show that $q_i^{n+1} = q_i^n$. The updated discharge q_i^{n+1} is given by (5.12), with $q_i^{n+\frac{2}{3}}$ defined by (5.9) and (5.8). Since $(\overline{h^\eta})_i^{n+1}$ is given by (5.17) and has been chosen to ensure $q_i^{n+1} = q_i^n$, the proof is concluded. □

6. Second-order MUSCL extension

We devote this section to a second-order extension based on a MUSCL technique (for instance, see [42, 43, 29, 30, 40]), to improve the space accuracy of the scheme. The MUSCL procedure involves a piecewise linear reconstruction, instead of piecewise constant, in the Godunov-type scheme. In addition, we use Heun's method to increase the time accuracy of the scheme.

6.1. The MUSCL reconstruction

The variables to be reconstructed are h, q and $h + Z$. Thus, note that the approximation of Z turns out to be time-dependent. For the sake of simplicity and conciseness in the notations, consider $w \in \{h, q, h+Z\}$. The reconstruction procedure consists in replacing the constant state w_i^n with a linear approximation, given in each cell $(x_{i-\frac{1}{2}}, x_{i+\frac{1}{2}})$ by

$$w_i^n(x) = w_i^n + (x - x_i)\,\sigma_i^n,$$

where σ_i^n is the limited slope of the linear reconstruction. A limiter is applied to this slope, in order to improve the stability of the scheme. Here, we have chosen the classical minmod limiter (the reader is referred for instance to [30] for more details regarding the use of slope limiters and a wider range of limiters). The limited slope σ_i^n is thus given by

$$\sigma_i^n = \text{minmod}\left(\frac{w_{i+1}^n - w_i^n}{\Delta x}, \frac{w_i^n - w_{i-1}^n}{\Delta x}\right),$$

where the minmod function is defined by

$$\text{minmod}(a,b) = \begin{cases} a & \text{if } |a| < |b| \text{ and } ab > 0, \\ b & \text{if } |a| > |b| \text{ and } ab > 0, \\ 0 & \text{if } ab \leq 0. \end{cases}$$

Thus, at the inner interfaces of the cell $(x_{i-\frac{1}{2}}, x_{i+\frac{1}{2}})$, the reconstructed variables are given by

$$w_i^- := w_i^n\left(x_i - \frac{\Delta x}{2}\right) = w_i^n - \frac{\Delta x}{2}\sigma_i^n, \tag{6.1a}$$

$$w_i^+ := w_i^n\left(x_i + \frac{\Delta x}{2}\right) = w_i^n + \frac{\Delta x}{2}\sigma_i^n. \tag{6.1b}$$

Since $w \in \{h, q, h+Z\}$, the reconstructed value of Z at the interfaces is computed from the reconstructed values of $h+Z$ and h at the interfaces.

Therefore, the updated states are given by the following three step scheme.

- Transport step:

$$h_i^{n+\frac{1}{3}} = h_i^n - \frac{\Delta t}{\Delta x}\left((f^h)_{i+\frac{1}{2}}^n - (f^h)_{i-\frac{1}{2}}^n\right), \tag{6.2a}$$

$$q_i^{n+\frac{1}{3}} = q_i^n - \frac{\Delta t}{\Delta x}\left((f^q)_{i+\frac{1}{2}}^n - (f^q)_{i-\frac{1}{2}}^n\right), \tag{6.2b}$$

  where $(f^h)_{i+\frac{1}{2}}^n := f^h(W_i^+, W_{i+1}^-)$ and $(f^q)_{i+\frac{1}{2}}^n := f^q(W_i^+, W_{i+1}^-)$ according to (5.5). The water height $h_i^{n+\frac{1}{3}}$ is then reconstructed within the cell $(x_{i-\frac{1}{2}}, x_{i+\frac{1}{2}})$, following (6.1), to get h_i^- and h_i^+.

- Topography step:

$$h_i^{n+\frac{2}{3}} = h_i^{n+\frac{1}{3}}, \tag{6.3a}$$

$$q_i^{n+\frac{2}{3}} = q_i^{n+\frac{1}{3}} + \Delta t (S^t)_i^{n+\frac{2}{3}}, \tag{6.3b}$$

$$(S^t)_i^{n+\frac{2}{3}} = \frac{1}{2}\left(\overline{S}^t(h_{i-1}^+, h_i^-, Z_{i-1}^+, Z_i^-) + \overline{S}^t(h_i^+, h_{i+1}^-, Z_i^+, Z_{i+1}^-)\right), \tag{6.3c}$$

  where $\overline{S}^t$ is defined by (4.2).

- Friction step:

$$h_i^{n+1} = h_i^{n+\frac{2}{3}}, \tag{6.4a}$$

$$q_i^{n+1} = \frac{\left((\overline{h^\eta})_i^{n+1}\right)^\eta q_i^{n+\frac{2}{3}}}{\left((\overline{h^\eta})_i^{n+1}\right)^\eta + k\,\Delta t\,|q_i^{n+\frac{2}{3}}|}, \tag{6.4b}$$

$$(\overline{h^\eta})_i^{n+1} = \frac{2\mu_i^{n+\frac{2}{3}}\mu_i^n}{\left(\overline{h^{-\eta}}\right)_{i-\frac{1}{2}}^{n+1} + \left(\overline{h^{-\eta}}\right)_{i+\frac{1}{2}}^{n+1}} + k\,\Delta t\,\mu_i^{n+\frac{2}{3}} q_i^n, \tag{6.4c}$$

where $(\overline{h^{-\eta}})_{i-\frac{1}{2}}^{n+1} := \overline{h^{-\eta}}(h_i^+, h_{i+1}^-)$, according to (3.23).

Finally, the scheme's time accuracy is improved by the use of the classical Heun's method (see [22]).

6.2. MOOD technique to recover the well-balance property

At this level, the designed MUSCL scheme is not well-balanced. Indeed, if W_i^n and W_{i+1}^n define a steady state, the reconstruction step (6.1) will provide reconstructed values W_i^+ and W_{i+1}^- that no longer define a steady state. Thus, the scheme will not be able to exactly preserve the initial steady state, but will provide a second-order approximation. To restore this essential property, we use a MOOD-like technique (see [13] for an overview of such techniques, and [7] for more recent applications). We suggest to introduce a convex combination between the reconstructed state and the non-reconstructed one (see [26] for related work). As a consequence, we adopt the following reconstruction:

$$w_i^- = (1-\theta_i^n)\,w_i^n + \theta_i^n\left(w_i^n - \frac{\Delta x}{2}\sigma_i^n\right) = w_i^n - \frac{\Delta x}{2}\sigma_i^n\theta_i^n, \tag{6.5a}$$

$$w_i^+ = (1-\theta_i^n)\,w_i^n + \theta_i^n\left(w_i^n + \frac{\Delta x}{2}\sigma_i^n\right) = w_i^n + \frac{\Delta x}{2}\sigma_i^n\theta_i^n, \tag{6.5b}$$

where $0 \le \theta_i^n \le 1$ is the parameter of the convex combination. If $\theta_i^n = 1$, the full MUSCL scheme is recovered. If $\theta_i^n = 0$, the states are not reconstructed and the first-order well-balanced scheme is used.

Now, we propose a suitable process to define the parameter θ_i^n. To that end, we first define

$$\Delta\psi_{i+\frac{1}{2}}^n = \frac{(q_{i+1}^n)^2}{h_{i+1}^n} - \frac{(q_i^n)^2}{h_i^n} + \frac{g}{2}\left((h_{i+1}^n)^2 - (h_i^n)^2\right) - \Delta x\overline{S}_{i+\frac{1}{2}}^t - \Delta x\overline{S}_{i+\frac{1}{2}}^f,$$

where $\overline{S}_{i+\frac{1}{2}}^t = \overline{S}^t(h_i^n, h_{i+1}^n, Z_i, Z_{i+1})$ and $\overline{S}_{i+\frac{1}{2}}^f = \overline{S}^f(h_i^n, h_{i+1}^n, q_i, q_{i+1})$, with $\overline{S}^t$ and $\overline{S}^f$ respectively defined by (4.2) and (3.28). Note that, from (4.4), $\Delta\psi_{i+\frac{1}{2}}^n$ vanishes when W_i^n and W_{i+1}^n define a steady state. Thus, from this quantity,

we define a function to evaluate the deviation with respect to the equilibrium, as follows:

$$\varphi_i^n = \left\| \begin{pmatrix} q_i^n - q_{i-1}^n \\ \Delta\psi_{i-\frac{1}{2}}^n \end{pmatrix} \right\|_2 + \left\| \begin{pmatrix} q_{i+1}^n - q_i^n \\ \Delta\psi_{i+\frac{1}{2}}^n \end{pmatrix} \right\|_2 .$$

Since $\Delta\psi_{i+\frac{1}{2}}^n$ vanishes when W_i^n and W_{i+1}^n define a steady state, this newly introduced quantity φ_i^n vanishes when W_{i-1}^n, W_i^n and W_{i+1}^n define a steady state. Let $M > m > 0$. We define the parameter of the convex combination θ_i^n as follows:

$$\theta_i = \begin{cases} 0 & \text{if } \varphi_i^n < m\,\Delta x \\ \dfrac{\varphi_i^n - m\Delta x}{M\Delta x - m\Delta x} & \text{if } m\,\Delta x \le \varphi_i^n \le M\,\Delta x \\ 1 & \text{if } \varphi_i^n > M\,\Delta x. \end{cases} \tag{6.6}$$

This definition of θ_i enforces the use of the MUSCL scheme if the states are far from defining a steady state, i.e. φ_i^n is large enough; the first-order well-balanced scheme is used if the equilibrium error φ_i^n is small enough. In addition, the closer the states are to the equilibrium, the more the convex combination will favor the first-order well-balanced scheme.

7. Numerical experiments

This last section is devoted to numerical tests, in one and two dimensions. We start by recalling the different schemes we shall test:

- the *explicit* scheme is (3.6) - (4.10);
- the *implicit* scheme is (5.8) - (5.9) - (5.12) - (5.17);
- the *MUSCL* scheme is (6.2) - (6.3) - (6.4) - (6.5).

In order to assess the properties of these schemes, we present three sets of numerical experiments. The first set assesses the well-balancedness of the scheme, by considering steady states at rest and moving steady states with topography and/or friction. The focus of the second set is the simulation of wet and dry dam-breaks, over a possibly complicated topography, and with a nonzero Manning coefficient k. Finally, the third set of experiments concerns simulations in two dimensions.

The constants will be chosen according to the following table.

Constant	Equation	Value
g	(1.1)	9.81
ε_λ	(3.3)	10^{-10}
ε	(3.29)	0

Table 1: Values of the constants within the numerical experiments.

Moreover, we will compute errors to make sure the schemes are indeed well-balanced. The L^1, L^2 and L^∞ errors for a bounded function w are computed as follows:

$$L^1 : \frac{1}{N}\sum_{i=1}^{N} |w_i - w_i^{ex}| \; ; \; L^2 : \sqrt{\frac{1}{N}\sum_{i=1}^{N} (w_i - w_i^{ex})^2} \; ; \; L^\infty : \max_{1\leq i\leq N} |w_i - w_i^{ex}|,$$

where w_i and w_i^{ex} are respectively the approximate and the exact solution at the point x_i and at the final physical time t_{end}, and N is the number of discretization cells. Finally, we recall that the CFL condition (3.5) gives the time step Δt at each iteration, as follows:

$$\Delta t \leq \frac{\Delta x}{2\Lambda}, \quad \text{where } \Lambda = \max_{i\in\mathbb{Z}} \left(\lambda^L_{i+\frac{1}{2}}, \lambda^R_{i+\frac{1}{2}}\right).$$

7.1. Verification of the well-balancedness

In this first set of experiments, we assess the well-balancedness of the scheme, i.e. its ability to exactly preserve and capture steady states. Recall that steady states are given by the equation (1.5), which prescribes a uniform discharge over the space domain, denoted q_0. First, we consider steady states at rest, i.e. $q_0 = 0$. Then, we consider moving steady states with a vanishing friction contribution, i.e. $k = 0$. Afterwards, steady states for the friction source term only are studied, that is to say we impose $q_0 \neq 0$ and $\partial_x Z = 0$. Finally, we consider steady states for both friction and topography, which are either analytic solutions in specific cases or steady states obtained by approximately solving (1.5).

7.1.1. Lake at rest steady states

We begin by lake at rest steady states, to assess the well-balancedness of the explicit, implicit and MUSCL schemes. In the three cases we consider, we have $q_0 = 0$ and $k = 10$. Since the friction contribution to the equations vanishes as soon as $q_0 = 0$, the smooth steady states are given by $\partial_x(h + Z) = 0$, i.e. the free surface stays uniform over the wet domain. We consider three different steady states at rest. All three of these experiments are performed with 200 discretization cells, over the domain $[0, 1]$ and until a final time $t_{end} = 1$s. The exact solution at rest is imposed at the boundaries. The initial conditions are $q(x) = 0$ and $h(x) + Z_i(x) = 2$, with topographies $(Z_i)_{i\in\{1,2,3\}}$ given by

$$\begin{aligned} Z_1(x) &= (1 - 2\,|2x - 1|)_+ \,; \\ Z_2(x) &= \mathbb{1}_{[\frac{1}{2},1]}(x); \\ Z_3(x) &= (4x - 1)\,\mathbb{1}_{[\frac{1}{2},1]}(x). \end{aligned}$$

These initial free surfaces are presented Figure 4. Note that Z_2 and Z_3 are discontinuous, and that the experiment where Z_3 is used involves a dry/wet transition. The results of the simulations with the three schemes are presented

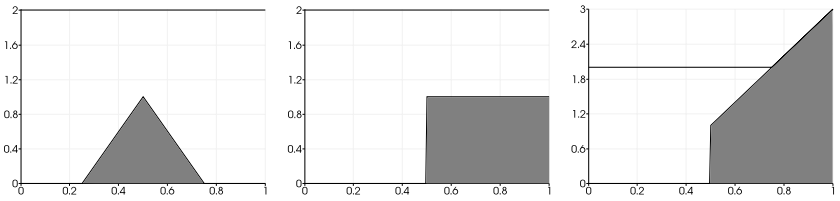

Figure 4: From left to right: free surfaces for the lake at rest experiments, with topographies given by Z_1, Z_2 and Z_3.

	$h+Z$			q		
	L^1	L^2	L^∞	L^1	L^2	L^∞
explicit	2.28e-16	2.92e-16	8.88e-16	1.31e-15	1.75e-15	4.81e-15
implicit	9.10e-16	9.19e-16	1.33e-15	1.45e-15	2.02e-15	5.30e-15
MUSCL	4.96e-16	6.78e-16	1.55e-15	5.18e-15	6.29e-15	1.39e-14

Table 2: Free surface and discharge errors for the steady state at rest experiment, with topography given by Z_1.

	$h+Z$			q		
	L^1	L^2	L^∞	L^1	L^2	L^∞
explicit	0	0	0	2.12e-16	6.09e-16	2.78e-15
implicit	0	0	0	2.08e-16	6.05e-16	2.78e-15
MUSCL	0	0	0	2.11e-16	6.18e-16	2.78e-15

Table 3: Free surface and discharge errors for the steady state at rest experiment, with topography given by Z_2.

	$h+Z$			q		
	L^1	L^2	L^∞	L^1	L^2	L^∞
explicit	7.99e-17	1.88e-16	6.66e-16	3.21e-16	5.32e-16	1.96e-15
implicit	9.55e-17	1.84e-16	6.66e-16	4.84e-16	7.38e-16	2.01e-15
MUSCL	0	0	0	0	0	0

Table 4: Free surface and discharge errors for the steady state at rest experiment, with topography given by Z_3.

in Tables 2 - 3 - 4. We used $C = +\infty$ in (4.3), and we took $m = 10^{-15}$ and $M = 10^{-14}$ in (6.6). Numerically, we set C as the upper bound of the double precision floating point numbers.

Tables 2 - 3 - 4 present the results of the three schemes at time $t_{end} = 1$s. The three schemes exactly preserve the lake at rest steady state, even in the cases of a discontinuous topography and a dry/wet transition.

7.1.2. Moving steady states for the topography only

Now, after [23], we consider moving steady states without friction, i.e. $k = 0$. Two experiments are carried out, the *subcritical flow* and the *transcritical flow without shock*. From now on, they will respectively be referred to as GM1 and GM2. Since we consider steady states without friction, they are governed by $q(x) = q_0$ and the equation (1.9). For smooth steady states, this equation can be rewritten as follows:

$$\partial_x \left(\frac{q_0^2}{2h^2} + g\,(h + Z) \right) = 0.$$

Note that the above equation states Bernoulli's principle, and reads

$$\frac{q_0^2}{2h^2} + g\,(h + Z) = H,$$

with H the total head, which is uniform throughout the domain. Since the schemes under consideration are well-balanced, they should capture these two moving steady states up to the machine precision, i.e. H and q should be uniform. Thus, we will compute the errors to these constants.

According to [23], the space domain is $[0, 25]$ and the topography is given by $Z(x) = \left(0.2 - 0.05(x - 10)^2\right)_+$. With subscripts 1 and 2 respectively corresponding to GM1 and GM2, the initial data are $q(x) = 0$ and $h(x) + Z(x) = h_i$, where $h_1 = 2$ and $h_2 = 0.66$. With $q_0 = 4.42$ for GM1 and $q_0 = 1.53$ for GM2, the boundary conditions are as follows.

- On the left boundary $x = 0$, a homogeneous Neumann boundary condition is prescribed for h, and we impose the Dirichlet boundary condition $q = q_0$.
- On the right boundary $x = 25$, we have a homogeneous Neumann boundary condition for q and h. Moreover, as soon as the flow becomes subcritical, the Dirichlet condition $h = h_i$ is imposed.

Note that these initial and boundary conditions ensure a transient state will be followed by a moving steady state with uniform discharge q_0.

Both these experiments are executed with 200 discretization cells, and are simulated until $t_{end} = 650$s for GM1 and $t_{end} = 175$s for GM2. For GM1, we take $C = +\infty$, $m = 10^{-10}$ and $M = 0.5$; for GM2, we take $C = 2.5$, $m = 10^{-10}$ and $M = 0.5$. The results of the explicit scheme are displayed Figures 5 - 6, and Tables 5 - 6 show the errors to the steady state for all three schemes.

Tables 5 and 6 indeed show that the steady state is captured up to the machine precision by the proposed schemes. Note that the presence of the transient state does not affect the ability of the scheme to preserve these two moving steady states.

7.1.3. Steady states for the friction source term

We now focus on the preservation of the friction-only steady states. Thus, we assume $q_0 \neq 0$ and a flat topography, i.e. $\partial_x Z = 0$. The smooth steady states are then given according to (1.10), or equivalently (2.2).

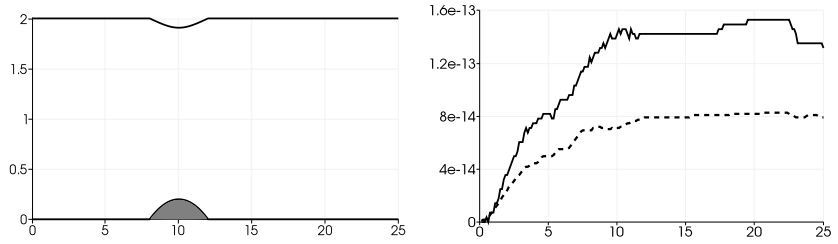

Figure 5: Left panel: free surface and topography for the GM1 experiment. Right panel: errors for the GM1 experiment using the explicit scheme; the solid line is the total head error and the dashed line is the discharge error.

	H			q		
	L^1	L^2	L^∞	L^1	L^2	L^∞
explicit	1.18e-13	1.25e-13	1.53e-13	6.65e-14	6.99e-14	8.26e-14
implicit	4.51e-14	5.37e-14	7.82e-14	7.55e-15	8.29e-15	1.42e-14
MUSCL	1.32e-14	1.44e-14	2.84e-14	2.28e-14	2.59e-14	3.82e-14

Table 5: Total head and discharge errors for the GM1 experiment, using the explicit, implicit and MUSCL schemes.

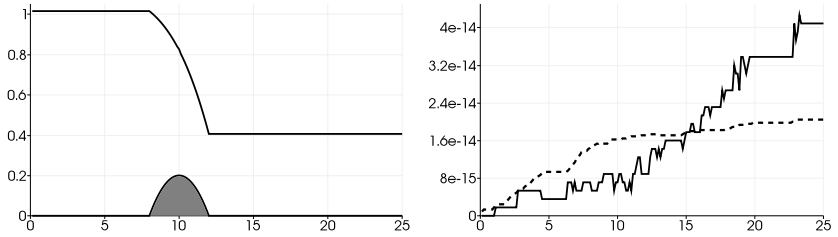

Figure 6: Left panel: free surface and topography for the GM2 experiment. Right panel: errors for the GM2 experiment using the explicit scheme; the solid line is the total head error and the dashed line is the discharge error.

	H			q		
	L^1	L^2	L^∞	L^1	L^2	L^∞
explicit	1.67e-14	2.13e-14	4.26e-14	1.47e-14	1.58e-14	2.04e-14
implicit	2.32e-14	2.67e-14	3.91e-14	1.31e-14	1.37e-14	1.67e-14
MUSCL	1.79e-14	2.23e-14	4.62e-14	1.06e-14	1.17e-14	2.18e-14

Table 6: Total head and discharge errors for the GM2 experiment, using the explicit, implicit and MUSCL schemes.

In Section 2, the water height for a smooth steady state was obtained by considering a zero of the nonlinear function ξ defined by (2.5). We consider the

subcritical branch of the steady state obtained by assuming $q_0 = -1$, $x_0 = 0$ and $h_0 = h_c$, with h_c defined by (2.6), over the domain $[0, 1]$. The Manning coefficient k is chosen equal to 1.

The first experiment concerns the preservation of this steady state. We take $q(x) = q_0$ and the exact height as initial conditions, and we impose the exact solutions as inhomogeneous Dirichlet boundary conditions. We use a mesh of 200 cells and compute the approximate solution until the final time $t_{end} = 1$s. Moreover, the parameters are taken as follows: $C = 10^{-3}$, $m = 10^{-14}$ and $M = 10^{-13}$. The results are presented Figure 7, and the errors to the steady state are displayed Table 7.

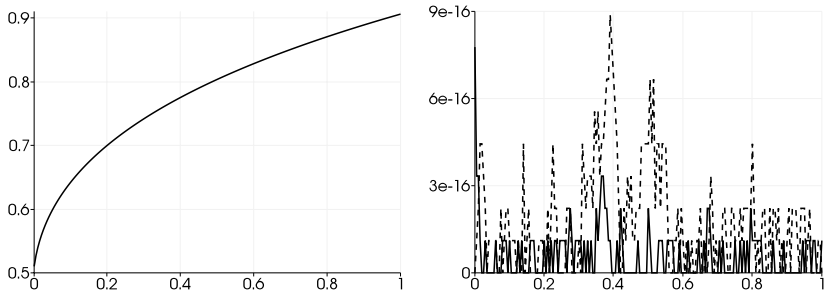

Figure 7: Left panel: initial height for the friction steady state. Right panel: height (solid line) and discharge (dashed line) errors to the steady state after 1s, with the explicit scheme.

	h			q		
	L^1	L^2	L^∞	L^1	L^2	L^∞
explicit	6.00e-17	1.09e-16	7.77e-16	1.81e-16	2.56e-16	8.88e-16
implicit	6.49e-17	1.15e-16	7.77e-16	2.91e-16	3.82e-16	9.99e-16
MUSCL	8.49e-17	1.33e-16	6.66e-16	2.42e-16	3.30e-16	8.88e-16

Table 7: Height and discharge errors with the three schemes for the friction steady state.

From Figure 7 and Table 7, we observe that this friction-only steady state is indeed preserved up to the machine precision by the three schemes.

The second experiment uses the same steady state as the first one, but with a perturbation, as shown in Figure 8. With h_{ex} the exact height, this perturbation is defined by choosing the initial water height as follows:

$$h(x) = \begin{cases} h_{ex}(x) + 0.2 & \text{if } x \in \left[\frac{3}{7}, \frac{4}{7}\right]; \\ h_{ex}(x) & \text{otherwise.} \end{cases}$$

The initial discharge is unperturbed, and taken equal to $q_0 = -1$ throughout the domain. The boundary conditions consist in the unperturbed exact solution. We

use the three schemes and 100 discretization cells for the numerical simulation. Moreover, we take $C = 10^{-3}$, $m = 10^{-14}$ and $M = 10^{-1}$. The computations are carried out until the final time $t_{end} = 9$s. Indeed, such a final time allows the perturbation to be dissipated and a steady state to be reached. In fact, this steady state is the original, unperturbed steady state. The results of the explicit scheme are presented Figure 8 and an error comparison with the unperturbed steady state is provided Table 8.

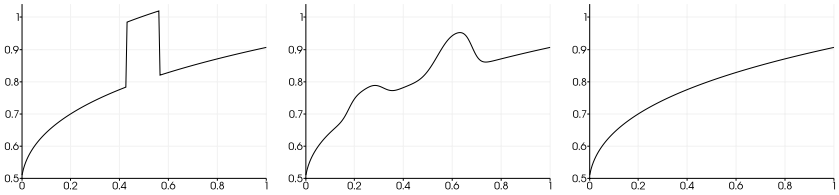

Figure 8: From left to right: water height for $t = 0$s, $t = 0.06$s and $t = 9$s, with the explicit scheme.

	h			q		
	L^1	L^2	L^∞	L^1	L^2	L^∞
explicit	7.42e-15	7.48e-15	8.55e-15	7.06e-15	8.32e-15	1.48e-14
implicit	7.06e-15	7.09e-15	8.10e-15	7.61e-15	8.81e-15	1.51e-14
MUSCL	8.40e-15	8.47e-15	1.04e-14	6.56e-15	7.52e-15	1.73e-14

Table 8: Height and discharge errors with the three schemes for the perturbed friction steady state.

Figure 8 shows that the perturbation is eventually dissipated and we recover the unperturbed steady state. This assertion is confirmed by the error analysis present Table 8, which shows that all three schemes recover the unperturbed steady state up to the machine precision.

Remark 3. We have carried out similar experiments with a supercritical branch instead of the subcritical branch. These experiments yielded similar conclusions. For the sake of conciseness, we do not present them here.

7.1.4. Steady states with both friction and topography

We conclude the verification of the well-balancedness with numerical experiments consisting in the preservation of steady states involving both topography and friction. Thus, $k \neq 0$, $\partial_x Z \neq 0$, and $q_0 \neq 0$. Steady states are therefore given by the full equation (1.5). Recall that this equation cannot be rewritten under an algebraic form. Thus, to find a general steady state solution, we have to numerically solve the equation (1.5).

We begin by considering two very specific cases, where the height or the free surface are constant, in order to obtain an analytical solution of (1.5).

First, assume $h(x) = h_0$, i.e. the water height is uniform and equal to h_0 in the whole space domain. Thus, (1.7) rewrites

$$gh_0\partial_x Z + kq_0|q_0|h_0^\eta = 0,$$

and we immediately obtain a relation characterizing the slope of the topography:

$$\partial_x Z = -\frac{kq_0|q_0|}{gh_0^{\eta+1}}. \tag{7.1}$$

This specific case is tested numerically by taking $h_0 = q_0 = 1$, $k = 10$, $Z(0) = 0$ and the slope of Z given by (7.1). The space domain is $[0, 1]$ and is discretized using 100 cells. The initial and boundary conditions are the exact solution. The computations are carried out with all three schemes, and we choose $t_{end} = 1$s. We take $C = +\infty$, $m = 10^{-14}$ and $M = 10^{-13}$. The results are presented Table 9.

	h			q		
	L^1	L^2	L^∞	L^1	L^2	L^∞
explicit	9.99e-18	3.68e-17	2.22e-16	9.99e-17	1.84e-16	6.66e-16
implicit	2.22e-17	5.21e-17	2.22e-16	9.99e-17	1.84e-16	6.66e-16
MUSCL	0	0	0	2.55e-17	6.75e-17	2.22e-16

Table 9: Height and discharge errors for the topography and friction steady state with constant height.

Table 9 shows that this topography and friction steady state with constant height is indeed exactly preserved by the three schemes.

To build another exact solution of (1.5), we assume $h + Z = H_0$ instead of $h = h_0$. We therefore have a constant free surface H_0 over the whole space domain $[0, 1]$. Note that (1.7) rewrites for smooth solutions with positive water height as follows:

$$-\frac{q_0^2}{h^2}\partial_x h + gh\partial_x(h + Z) + \frac{kq_0|q_0|}{h^\eta} = 0.$$

Since the free surface $h + Z$ is constant, the above relation rewrites

$$h^{\eta-2}\partial_x h = k\mu_0, \tag{7.2}$$

where $\mu_0 = \mathrm{sgn}(q_0)$. For $x \in [0, 1]$, integrating (7.2) over $[0, x]$ provides an expression of h that depends on the initial condition $h_0 := h(0)$, namely:

$$h^{\eta-1} = h_0^{\eta-1} + (\eta - 1)\, k\mu_0 x. \tag{7.3}$$

Note that (7.3) defines an expression of the height that may become non-positive for some x. Thus, we choose the constants k, q_0 and h_0 such that h is positive over the whole domain $[0, 1]$. In the simulation, we set $k = q_0 = h_0 = 1$.

Equipped with the water height, we define the topography by setting $Z = H_0 - h$. We discretize the space domain with 100 cells and use the three schemes to carry out the simulation until the time $t_{end} = 1$s. We take $C = +\infty$, $m = 10^{-13}$ and $M = 10^{-12}$. An error comparison of the three schemes is displayed Table 10.

	h			q		
	L^1	L^2	L^∞	L^1	L^2	L^∞
explicit	4.23e-15	4.48e-15	6.66e-15	3.06e-14	3.07e-14	3.60e-14
implicit	1.31e-16	2.00e-16	6.66e-16	1.45e-15	1.83e-15	4.88e-15
MUSCL	8.88e-17	1.57e-16	4.44e-16	4.46e-16	6.81e-16	2.22e-15

Table 10: Height and discharge errors for the topography and friction steady state with constant free surface.

The results presented Table 10 show that the steady state is preserved up to the machine precision by the explicit, implicit and MUSCL schemes.

Finally, we derive a steady state for the shallow-water equations with topography and friction, without considering a constant height or free surface. Thus, we approximately solve the discretization (4.4) of the full equilibrium relation (1.7). First, we set $k = 0.01$ and choose $[0, 1]$ to be the space domain. Moreover, the topography is given by

$$Z(x) = \frac{1}{2}\frac{e^{\cos(4\pi x)} - e^{-1}}{e^1 - e^{-1}}.$$

We set $q = q_0$ throughout the domain. The equation (4.4) is then approximately solved using Newton's method, imposing $h(0) = 0.3$. This procedure allows us to define the water height over the whole domain. This steady state ${}^t(h, q)$ is then chosen as the initial and boundary conditions for this experiment. We take 100 discretization cells, $C = +\infty$, $m = 10^{-13}$ and $M = 10^{-12}$. The numerical simulation of this experiment is done using all three schemes, and runs until a final physical time $t_{end} = 1$s. The results of the explicit scheme are presented Figure 9 and the errors to the steady state are displayed Table 11.

	h			q		
	L^1	L^2	L^∞	L^1	L^2	L^∞
explicit	3.54e-16	4.49e-16	1.11e-15	1.66e-15	2.16e-15	3.55e-15
implicit	5.73e-16	8.99e-16	3.00e-15	5.07e-16	6.29e-16	1.55e-15
MUSCL	3.52e-17	5.40e-17	1.67e-16	3.75e-16	4.85e-16	1.33e-15

Table 11: Height and discharge errors with the three schemes for the topography and friction steady state.

Figure 9 shows that the explicit scheme exactly preserves this topography and friction steady state. Moreover, Table 11 shows that both other schemes also exactly preserve such a steady state.

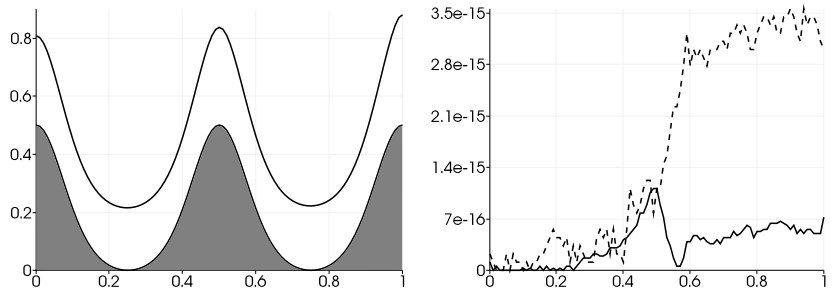

Figure 9: Left panel: initial height for the topography and friction steady state. Right panel: height (solid line) and discharge (dashed line) errors to the steady state with the explicit scheme.

The very last experiment in the well-balancedness assessment focuses on a perturbation of the aforementioned steady state. We denote by $h_{ex}(x)$ the water height of the previous topography and friction steady state. The initial water height of this last experiment is then given by

$$h(x) = \begin{cases} h_{ex}(x) + 0.05 & \text{if } x \in \left[\frac{2}{7}, \frac{3}{7}\right] \bigcup \left[\frac{4}{7}, \frac{5}{7}\right], \\ h_{ex}(x) & \text{otherwise,} \end{cases}$$

and the discharge is defined by

$$q(x) = \begin{cases} q_0 + \frac{1}{2} & \text{if } x \in \left[\frac{2}{7}, \frac{3}{7}\right] \bigcup \left[\frac{4}{7}, \frac{5}{7}\right], \\ q_0 & \text{otherwise.} \end{cases}$$

The unperturbed steady state is prescribed as the boundary conditions. For this numerical experiment, the domain $[0, 1]$ is discretized with 100 cells, and the simulation runs until the perturbation has been dissipated and the unperturbed steady state has been recovered. The final physical time we choose for these conditions to be met is $t_{end} = 2$s. Moreover, we set the parameters as $C = +\infty$, $m = 10^{-15}$ and $M = 0.05$. The evolution of the perturbation with the explicit scheme is presented Figure 10. Then, in Table 12, we present the errors to the original unperturbed steady state when the physical time is elapsed.

Figure 10 and Table 12 show that the scheme indeed allows to recover the original unperturbed steady state. This experiment emphasizes the ability of the three schemes to exactly capture a steady state, even after a perturbation.

7.2. Dam-break test cases

Now, we focus on dam-break numerical experiments. In these experiments, we consider a dam located at $x = x_D$ that instantly breaks at $t = 0$s, thus releasing the water it was holding. Such a dam-break experiment has initial data $W_L = {}^t(h_L(x), 0)$ if $x \leq x_D$ and $W_R = {}^t(h_R(x), 0)$ if $x > x_D$. The topography function Z and the Manning coefficient k are different in each experiment.

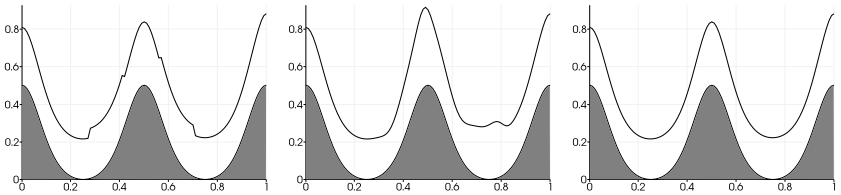

Figure 10: From left to right: water height for $t = 0$s, $t = 0.015$s and $t = 2$s, with the explicit scheme.

	h			q		
	L^1	L^2	L^∞	L^1	L^2	L^∞
explicit	5.10e-16	7.09e-16	2.44e-15	2.20e-15	2.92e-15	5.33e-15
implicit	4.85e-16	7.97e-16	2.72e-15	9.73e-16	1.15e-15	2.78e-15
MUSCL	6.46e-16	9.40e-16	3.50e-15	1.71e-15	2.23e-15	4.22e-15

Table 12: Height and discharge errors with the three schemes for the perturbed topography and friction steady state.

7.2.1. Wet dam-break

The first dam-break experiment under consideration is a wet dam-break. Here, the topography is given by $Z(x) = \cos^2(2\pi x)/2$ and the Manning coefficient is $k = 1$. The space domain is $[0, 1]$ and the dam is located at $x_D = 0.5$. We prescribe homogeneous Neumann boundary conditions at both boundaries. The initial data is $h_L(x) + Z(x) = 2$ and $h_R(x) + Z(x) = 1$. The results, obtained using 100 discretization cells and $t_{end} = 0.05$s, are displayed Figure 11. For this simulation, we choose $C = 10$, $m = 10^{-6}$ and $M = 10^{-1}$. The goal of this experiment is to compare the three schemes at our disposal to a reference solution, obtained using the MUSCL scheme with 10^4 discretization cells.

The three schemes yield a correct approximation of the reference solution. The explicit and the implicit schemes yield very close solutions, while the MUSCL scheme provides a better approximation of the reference solution.

An important remark we highlight is that the free surface yet untouched by the rarefaction wave or the shock wave should be unperturbed. This means that $h(x) + Z(x) = 2$ and $q(x) = 0$ for all x inferior to the position of the head of the rarefaction wave, and $h(x) + Z(x) = 1$ and $q(x) = 0$ for all x superior to the position of the shock wave. This behavior corresponds to a lake at rest configuration in the regions untouched by the waves. This lake at rest behavior is exactly preserved by the explicit and implicit schemes. The MUSCL scheme, equipped with the correction (6.5), also exactly preserves this configuration. This experiment showcases the relevance of the convex combination procedure involved in the MUSCL scheme, to preserve steady states while still ensuring a better approximation of the exact solution.

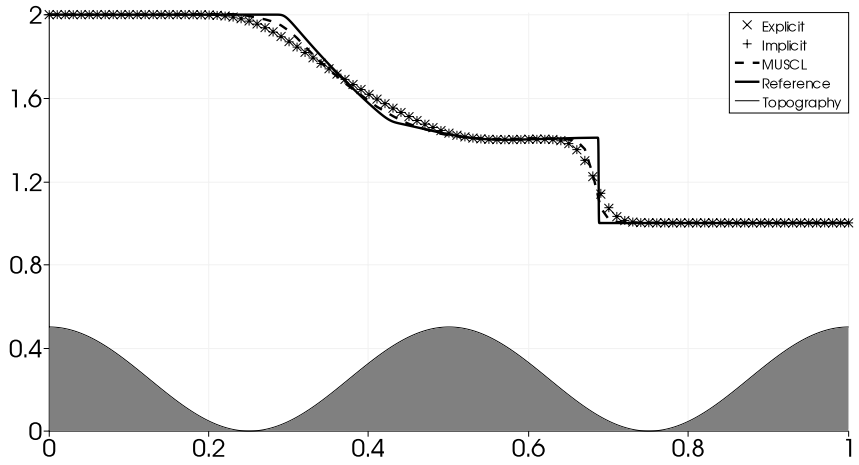

Figure 11: Free surface observed at the final physical time with the three schemes, for the wet dam-break experiment.

7.2.2. Dry dam-break

Now, we consider a dry dam-break. The topography is still given by $Z(x) = \cos^2(2\pi x)/2$ and the Manning coefficient is now $k = 10$. The initial data is $h_L(x) + Z(x) = 2$ and $h_R(x) = 0$. The space domain is $[0, 1]$ and the dam is located at $x_D = 0.5$. Moreover, the boundaries at $x = 0$ and $x = 1$ are equipped with homogeneous Neumann boundary conditions. We use 100 discretization cells and display the results Figure 12 at time $t_{end} = 0.05$s. We choose the constants $C = 7.5$, $m = 10^{-6}$ and $M = 10^{-1}$. We use the implicit and MUSCL schemes. Indeed, the explicit scheme present instabilities when dealing with dry/wet transitions. We also provide a reference solution for comparison purposes, obtained with the MUSCL scheme using 10^4 discretization cells.

The reference solution is once again correctly approximated by the two schemes, and the MUSCL scheme provides a better approximation of the solution than the implicit scheme. We make the same important remark concerning the preservation of the lake at rest behavior before the head of the rarefaction wave.

7.2.3. Dry dam-break with two bumps

This last dry dam-break experiment presents a more complicated topography, with two bumps. The space domain is $[0, 5]$ and we choose to use 10^4 discretization cells with the MUSCL scheme to have a relevant simulation. The two boundaries at $x = 0$m and $x = 5$m are solid walls. The topography is defined by

$$Z(x) = \frac{1}{2}\left(1 - \frac{(x-5/2)^2}{1/25}\right)_+ + 2\left(1 - \frac{(x-4)^2}{1/25}\right)_+,$$

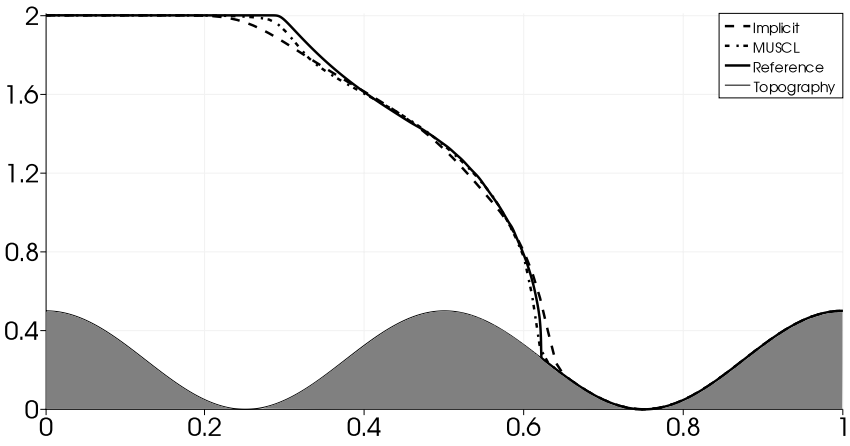

Figure 12: Free surface observed at the final physical time with the implicit and MUSCL schemes, for the dry dam-break experiment.

and indeed consists in two quadratic bumps, a smaller one followed by a larger one. The dam is located at $x_D = 0.7$m, breaks at $t = 0$s, and contains an initial water height $h_L = 6$m. The domain $x > x_D$ contains no water, i.e. $h_R = 0$. We choose a Manning coefficient k equal to 1. Figure 13 shows that the initial water height is significantly larger than the bumps. Indeed, we elected to have a larger mass of water whose energy is important enough not to be completely dissipated by the bottom friction. We choose $C = 0.1$, $m = 10^{-5}$ and $M = 10^{-1}$.

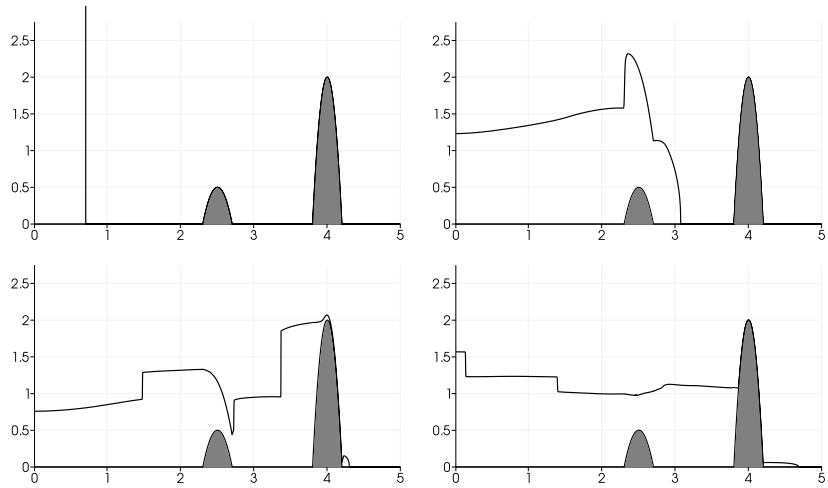

Figure 13: Free surface for the double bump test case at different times: from left to right and top to bottom, the solution is observed at times 0s, 0.38s, 0.74s and 1.70s.

7.3. 2D simulations

The subsection is devoted to experiments in two space dimensions. We begin by stating the shallow-water equations with topography and friction for two-dimensional geometries:

$$\begin{cases} \partial_t h + \partial_x p + \partial_y q & = & 0, \\ \partial_t p + \partial_x \left(\dfrac{p^2}{h} + \dfrac{1}{2} g h^2 \right) + \partial_y \left(\dfrac{pq}{h} \right) & = & -gh\partial_x Z - kpDh^{-\eta}, \\ \partial_t q + \partial_x \left(\dfrac{pq}{h} \right) + \partial_y \left(\dfrac{q^2}{h} + \dfrac{1}{2} g h^2 \right) & = & -gh\partial_y Z - kqDh^{-\eta}, \end{cases} \tag{7.4}$$

where p is the discharge in the x direction, q is the discharge in the y direction, and D is the Euclidean norm of the discharge vector, i.e. $D = \sqrt{p^2 + q^2}$. We rewrite (7.4) under the following condensed form:

$$\partial_t W + \partial_x f(W) + \partial_y g(W) = s(W),$$

where the definitions of W, f, g and s can easily be inferred from (7.4).

The numerical approximation involves a uniform Cartesian grid, made of square cells with sides $\Delta x = \Delta y$. For the 2D simulations, we will consider 2D variants of the implicit and MUSCL scheme, by applying the 1D strategy detailed in Section 5 and Section 6 in both directions, horizontal and vertical, of each square cell. This process involves exactly solving the initial value problem (5.10), related to the contribution of the friction only. However, this initial value problem is modified in two dimensions. Indeed, we have to solve

$$\begin{cases} \dfrac{dh}{dt} = 0, \\ \dfrac{dp}{dt} = -k(h_{i,j}^{n+1})^{-\eta} p \sqrt{p^2 + q^2}, \\ \dfrac{dq}{dt} = -k(h_{i,j}^{n+1})^{-\eta} q \sqrt{p^2 + q^2}, \end{cases} \quad \text{with initial data} \quad \begin{cases} h(0) = h_{i,j}^{n+\frac{2}{3}}, \\ p(0) = p_{i,j}^{n+\frac{2}{3}}, \\ q(0) = q_{i,j}^{n+\frac{2}{3}}. \end{cases} \tag{7.5}$$

We immediately see that $h_{i,j}^{n+1} = h_{i,j}^{n+\frac{2}{3}}$. For the sake of simplicity in the notations, we set $C = -k(h_{i,j}^{n+1})^{-\eta} < 0$, $p_n = p_{i,j}^{n+\frac{2}{3}}$ and $q_n = q_{i,j}^{n+\frac{2}{3}}$. Thus, (7.5) rewrites as the following initial value problem:

$$\begin{cases} p' = Cp\sqrt{p^2 + q^2}, \\ q' = Cq\sqrt{p^2 + q^2}, \end{cases} \quad \text{with initial data} \quad \begin{cases} p(0) = p_n, \\ q(0) = q_n. \end{cases}$$

The exact solution to this system is:

$$p(t) = \frac{p_n h_{i,j}^{n+1}}{h_{i,j}^{n+1} + kt\sqrt{p_n^2 + q_n^2}} \quad \text{and} \quad q(t) = \frac{q_n h_{i,j}^{n+1}}{h_{i,j}^{n+1} + kt\sqrt{p_n^2 + q_n^2}}.$$

Therefore, the friction step of the implicit procedure yields the following updated discharges:

$$p_{i,j}^{n+1} = \frac{p_{i,j}^{n+\frac{2}{3}}(h_{i,j}^{n+1})^{\eta}}{(h_{i,j}^{n+1})^{\eta} + k\Delta t\sqrt{(p_{i,j}^{n+\frac{2}{3}})^2 + (q_{i,j}^{n+\frac{2}{3}})^2}},$$
$$q_{i,j}^{n+1} = \frac{q_{i,j}^{n+\frac{2}{3}}(h_{i,j}^{n+1})^{\eta}}{(h_{i,j}^{n+1})^{\eta} + k\Delta t\sqrt{(p_{i,j}^{n+\frac{2}{3}})^2 + (q_{i,j}^{n+\frac{2}{3}})^2}}.$$

The quantity $(h_{i,j}^{n+1})^{\eta}$ is then replaced with the average given by (5.17), taken in the x direction for $p_{i,j}^{n+1}$ and in the y direction for $q_{i,j}^{n+1}$.

Such a 2D scheme will be able to exactly preserve the 1D steady states taken in the x direction or the y direction. Moreover, the splitting procedure allows simulating dry/wet interfaces. We use this 2D scheme for the simulations of three relevant situations. First, we focus on a dry dam-break with two bumps, which is a 2D version of the experiment presented Section 7.2.3. The next experiment is a partial dam-break, and the last experiment represents an urban topography.

7.3.1. 2D dry dam-break with two bumps

The first 2D experiment is a dry dam-break with a topography presenting two bumps. It is heavily inspired from an experiment presented in [8], which did not include the friction source term. The Manning coefficient is $k = 0.1$, and the topography function is given by

$$Z(x,y) = \frac{1}{2}\left(1 - 25\left(\left(x - \frac{5}{2}\right)^2 + \left(y - \frac{1}{2}\right)^2\right)\right)_+ + 2\left(1 - 25\left((x-4)^2 + \left(y - \frac{1}{2}\right)^2\right)\right)_+.$$

The space domain is $[0,5]\times[0,1]$. The initial discharge is zero in both directions, i.e. $p(x,y,0) = q(x,y,0) = 0$, and the initial water height is given by

$$h(x,y,0) = \begin{cases} 6 & \text{if } x < 0.7, \\ 0 & \text{otherwise.} \end{cases}$$

In addition, we prescribe wall boundary conditions, that is to say we impose $p(0,y,t) = p(5,y,t) = 0$ and $q(x,0,t) = q(x,1,t) = 0$ for all x, y and t.

The simulation runs until a physical time $t_{end} = 1.35$s with the MUSCL scheme, using $C = 1$, $m = 10^{-5}$ and $M = 25$. We take 288000 discretization cells (1200 in the x direction and 240 in the y direction). The results are presented Figures 14 - 15.

This experiment has been carried out to make sure that the numerical scheme still behaves correctly in two space dimensions and in the presence of dry/ wet

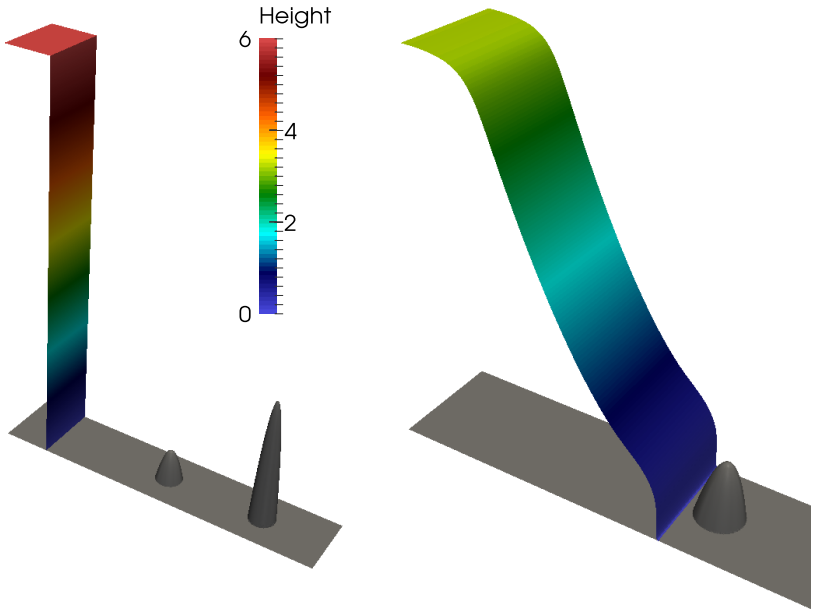

Figure 14: Left panel: initial condition of the 2D dam-break over a double bump experiment. Note that the same color scale for the water height is used Figures 14 - 15, and the solid gray color represents the topography. Right panel: approximate solution at $t = 0.15$s, just before the water hits the first bump. Note the shape of the front of the water, due to the nonzero bottom friction.

transition. We recover a numerical solution involving the friction source term, which can be compared to the numerical solution without friction presented in [8]. In addition, this 2D experiment is similar to the 1D double bump experiment we presented on Figure 13. Indeed, the behavior of the water before it comes into contact with the first bump should be the same in both experiments. As expected, we obtain similar results in 1D and 2D.

7.3.2. Partial dam-break

Next, we focus on a partial dam-break (see for instance [37, 14]). This experiment concerns a dam that has partially broken, leaving a corridor where the water flows. We consider the space domain $[-100, 100] \times [-100, 100]$. The dam is located at the middle of the domain, in the x direction, and is 10m wide and 100m high. It breaks in the middle, over a length of 80m. Thus, we take the following topography function:

$$Z(x,y) = \begin{cases} 1 & \text{if } x \leq -5, \\ 0 & \text{if } x \leq 5, \\ 0.1(5-x) & \text{if } -5 < x < 5 \text{ and } -40 < y < 40, \\ 100 & \text{if } -5 < x < 5 \text{ and } y \in [-100, -40] \cup [40, 100]. \end{cases}$$

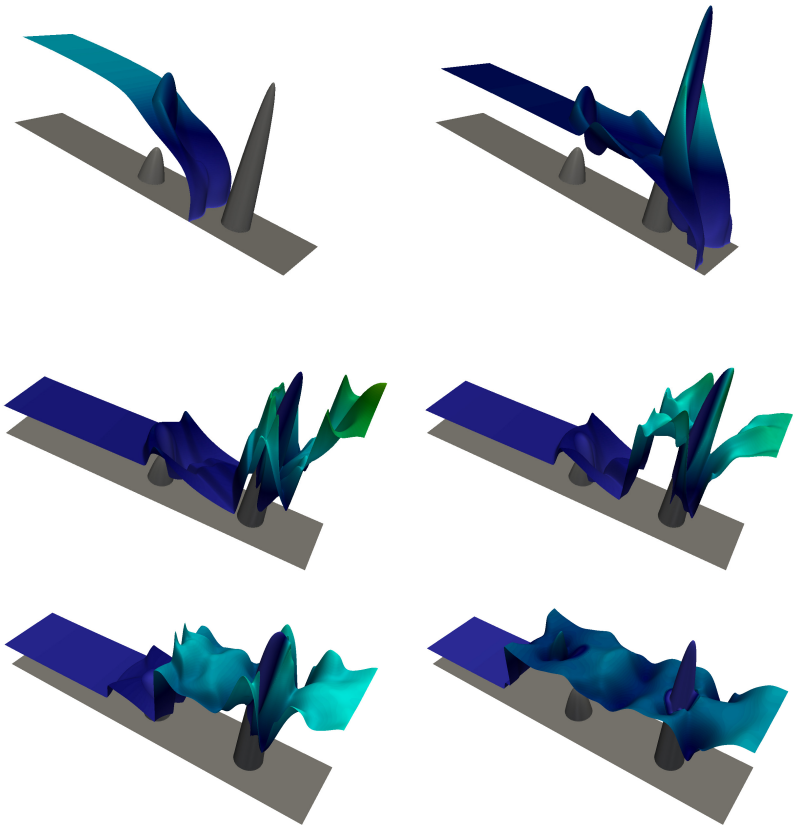

Figure 15: From left to right and top to bottom: approximate solution of the 2D dam-break over a double bump experiment, displayed at times $t = 0.3$s, $t = 0.45$s, $t = 0.75$s, $t = 0.9$s, $t = 1.05$s and $t = 1.35$s.

As in the previous dam-break experiment, we take $p(x, y, 0) = 0$ and $q(x, y, 0) = 0$. Moreover, we define the initial water height by:

$$h(x, y, 0) = \begin{cases} 10 & \text{if } x < -5, \\ 5 & \text{otherwise.} \end{cases}$$

From such initial data, we present two simulations. The first one is the case without friction, i.e. $k = 0$, and for the second one we choose a nonzero Manning coefficient $k = 2$. In both cases, homogeneous Neumann boundary conditions are prescribed on all the boundaries. We choose $t_{end} = 7$s. The numerical simulation of this experiment is carried out with the implicit and the MUSCL scheme on 202500 cells (450 in each direction). The results are displayed Figure 16 without friction, and Figure 17 with friction. Note that, on these figures, the display of the free surface is clipped when $Z > 10$, in order to have a clearer display of the numerical results, that is not impacted by the tall

remains of the dam.

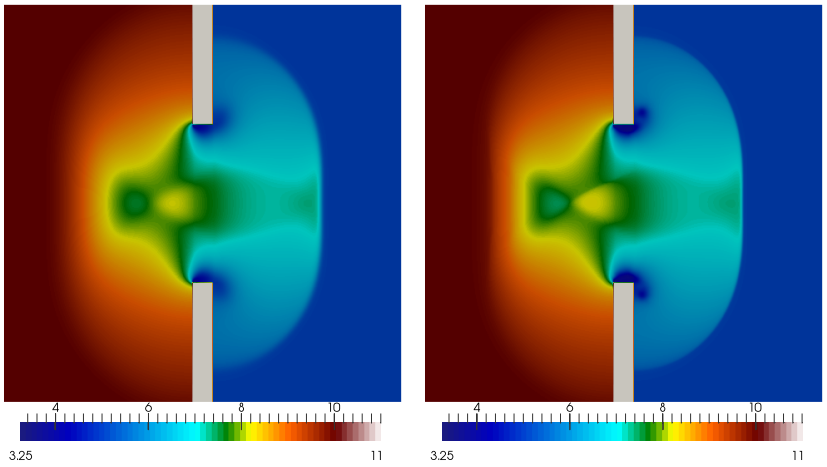

Figure 16: Approximate free surface for the partial dam-break experiment without friction. Left panel: implicit scheme; right panel: MUSCL scheme.

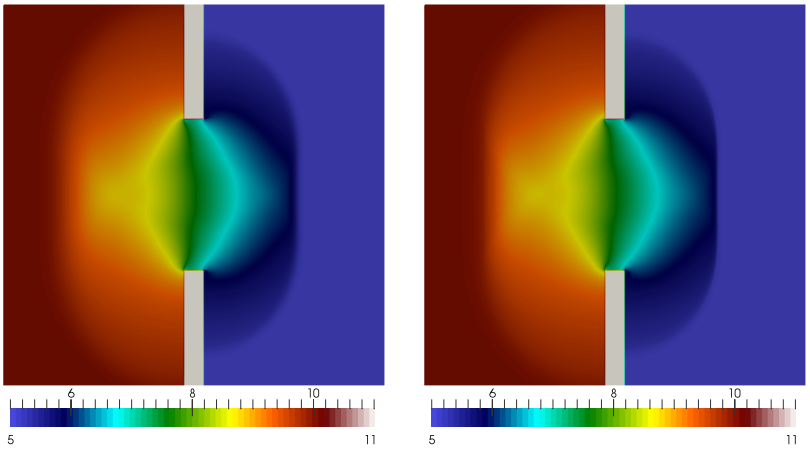

Figure 17: Approximate free surface for the partial dam-break experiment with nonzero friction. Left panel: implicit scheme; right panel: MUSCL scheme.

Figure 16 shows that, when no friction is present, vortices appear at both tips of the dam. However, as evidenced by Figure 17, these vortices no longer exist when the friction is nonzero. Both behaviors are exhibited with the implicit and MUSCL schemes. In addition, the tip of the left shock wave has traveled further on Figure 16 than on Figure 17. This behavior is consistent with the fact that the friction tends to slow down the movement of the water.

Now, to conclude the analysis of this experiment, we introduce (x_T, y_T) and (x_B, y_B). They are, respectively, the points where the top and bottom vortices

are the deepest when $k = 0$. In Table 13, we present the height at these two points, obtained with the implicit and MUSCL schemes, and considering $k = 0$ or $k = 2$. In addition, we display in this table the approximate position x_S of the left shock wave in the four cases under consideration, where it crosses the line $y = 0$.

	h_T	h_B	x_S
implicit, $k = 0$	2.81	2.81	59.3
implicit, $k = 2$	6.08	6.08	53.9
MUSCL, $k = 0$	2.33	2.30	59.8
MUSCL, $k = 2$	5.86	5.86	52.5

Table 13: Height at the positions of the two vortices and position of the left shock wave. We have set $h_T = h(x_T, y_T, t_{end})$ and $h_B = h(x_B, y_B, t_{end})$.

7.3.3. Urban topography

The last 2D experiment is a simulation of a city being hit by a wave. We consider the space domain $[0, 1000] \times [0, 1000]$. The topography consists in an upwards slope leading to a flat surface, upon which buildings are placed. Disregarding the buildings, the bottom has the following topography:

$$Z(x, y) = \begin{cases} x/50 & \text{if } x < 500, \\ 10 & \text{otherwise.} \end{cases}$$

The 100 meters high buildings occupy the flat part of the topography, i.e. buildings are only present for $x > 500$. Figure 18 displays the shapes of the buildings.

The initial conditions are $W(x, y, 0) = 0$ for all x and y in the space domain. Indeed, the boundary conditions help create the flood and the wave that hits the city. We prescribe homogeneous Neumann boundary conditions for each boundary of the domain, except the left boundary, where a time-dependent boundary condition the x-discharge p is applied, as follows:

$$\begin{cases} p(0, y, t) = 15 & \text{if } t < 350, \\ \partial_x p(0, y, t) = 0 & \text{otherwise.} \end{cases} \tag{7.6}$$

Such a boundary condition creates water that fills the sloping part of the topography and creates a wave that hits the city. We consider a nonzero Manning coefficient $k = 1$ and a final time $t_{end} = 850$s. The simulation is run using the MUSCL scheme, and we take $C = 10^{-2}$, $m = 10^{-5}$ and $M = 1$. We use a uniform Cartesian mesh of 202500 cells (450 in each direction). The results of the numerical simulation are displayed Figures 19 - 20 - 21 - 22.

The left panel of Figure 19 shows the wave created by the Dirichlet boundary condition arriving on the city. Because of the friction, this wave presents a rather steep front. On the right panel of Figure 19, the wave has hit the first buildings located at the south of the city. Note that the space between the first

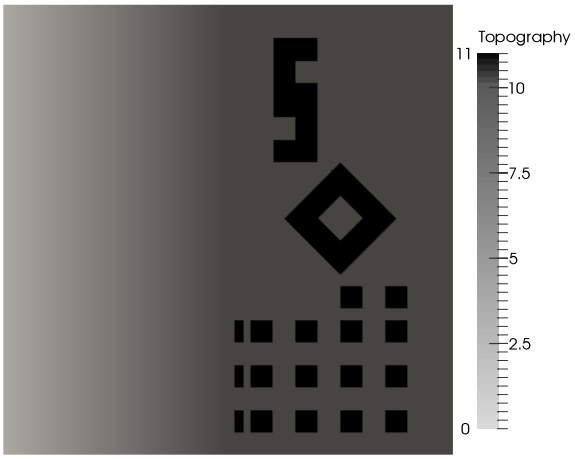

Figure 18: Topography for the city experiment. The buildings are actually 100 meters high, and are represented in black in this figure. One can see the upwards slope on the left, leading to the city itself.

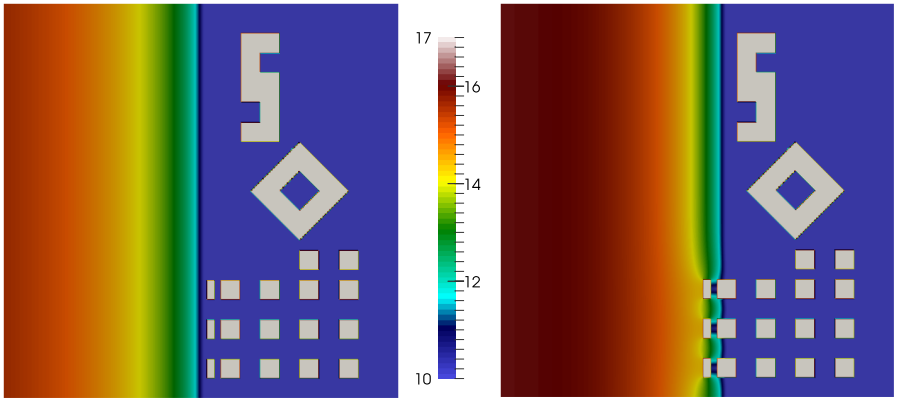

Figure 19: Free surface for the city experiment at $t = 314$s (left panel) and $t = 369$s (right panel). Note that the same color scale will be used in Figures 19 - 20 - 21 - 22, with the buildings being 100 meters high and the dry areas being blue.

two columns of buildings is still dry. Also note that, as per (7.6), the boundary condition imposed on the x-discharge p is now a homogeneous Neumann boundary condition, and no more water is injected into the domain.

The left panel of Figure 20 displays the wave about to hit the square building located at the middle of the city. As expected, between the southern buildings, the wave is slowed down. On the right panel of Figure 20, the wave has reflected on the southwestern side of the square building, and has thus moved faster towards the buildings to the south.

On the left panel of Figure 21, the waves reflected from the square buildings

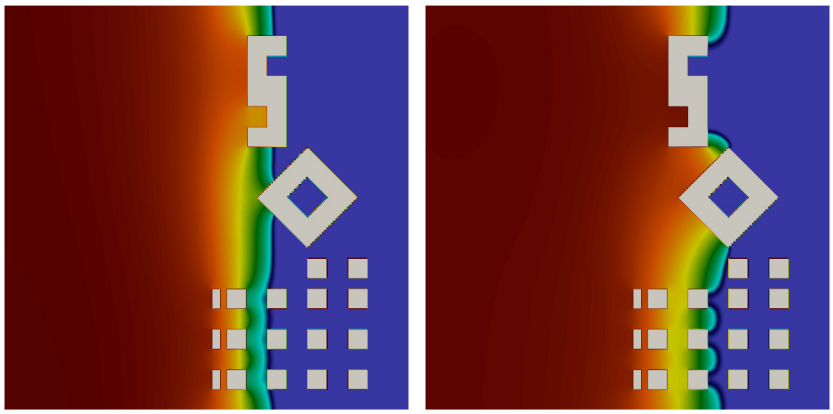

Figure 20: Free surface for the city experiment at $t = 451$s (left panel) and $t = 520$s (right panel).

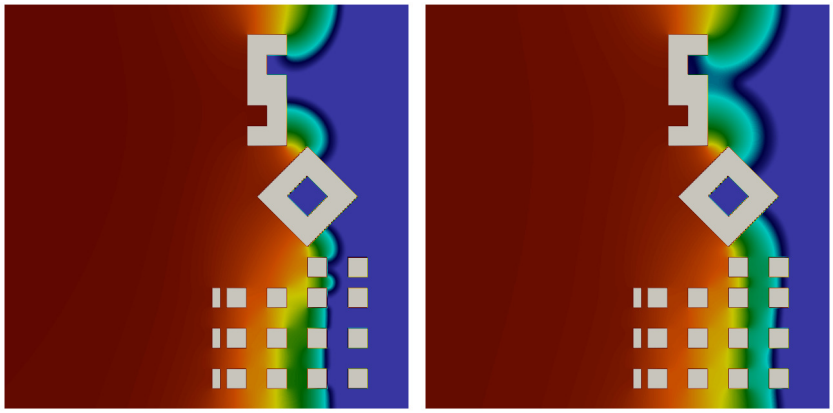

Figure 21: Free surface for the city experiment at $t = 603$s (left panel) and $t = 685$s (right panel).

are moving south and north. Moreover, the back of the "S"-shaped building will soon be flooded. This flooding has started to happen on the right panel of Figure 21, with only a small area still dry.

Figure 22 displays the final phases of the flooding of the city. Note that the southern buildings are mostly uniformly flooded and that the inner courtyard of the square building is still dry. Moreover, the water at the back of the "S"-shaped building is less deep than at other points of the same vertical line.

8. Conclusion

In this work, we have first studied smooth steady states for the shallow-water equations with friction only. Then, we have proposed a Godunov-type scheme

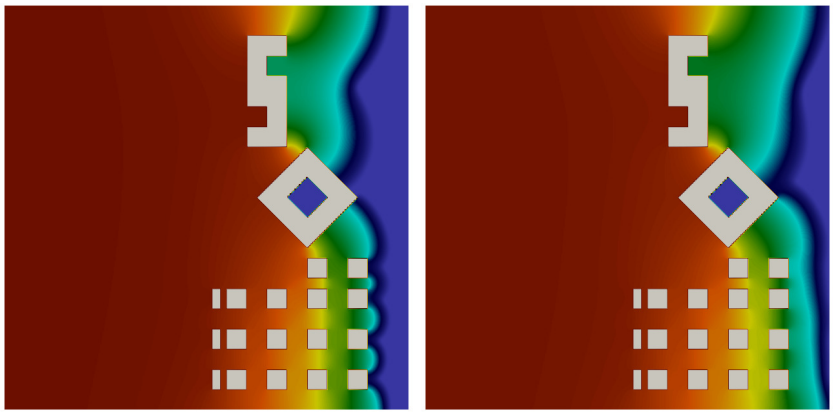

Figure 22: Free surface for the city experiment at $t = 767$s (left panel) and $t = 850$s (right panel).

for the same equations that is well-balanced. This scheme has then been extended to add the topography contribution as well as the positivity preservation. Afterwards, we have proposed a semi-implicit scheme to deal with dry/wet interfaces, followed by a well-balanced second-order extension. Finally, we have proposed several one-dimensional and two-dimensional numerical experiments.

Acknowledgments

C. Berthon, F. Foucher and V. Michel-Dansac would like to thank the ANR-12-IS01-0004-01 GEONUM for financial support. S. Clain would like to thank the FCT-ANR/MAT-NAN/0122/2012 grant for financial support.

References

[1] E. Audusse, F. Bouchut, M.-O. Bristeau, R. Klein, and B. Perthame. A fast and stable well-balanced scheme with hydrostatic reconstruction for shallow water flows. *SIAM J. Sci. Comput.*, 25(6):2050–2065, 2004.

[2] E. Audusse, C. Chalons, and P. Ung. A simple well-balanced and positive numerical scheme for the shallow-water system. *Commun. Math. Sci.*, 13(5):1317–1332, 2015.

[3] A. Bermudez and M. E. Vazquez. Upwind methods for hyperbolic conservation laws with source terms. *Comput. & Fluids*, 23(8):1049–1071, 1994.

[4] C. Berthon and C. Chalons. A fully well-balanced, positive and entropy-satisfying Godunov-type method for the shallow-water equations. 2013.

[5] C. Berthon, C. Chalons, S. Cornet, and G. Sperone. Fully well-balanced, positive and simple approximate Riemann solver for shallow-water equations. *Proceedings of HYP2014 international conference*, 2014.

[6] C. Berthon, A. Crestetto, and F. Foucher. A well-balanced finite volume scheme for a mixed hyperbolic/parabolic system to model chemotaxis. 2015.

[7] C. Berthon and V. Desveaux. An entropy preserving MOOD scheme for the Euler equations. *Int. J. Finite Vol.*, 11:39, 2014.

[8] C. Berthon and F. Foucher. Efficient well-balanced hydrostatic upwind schemes for shallow-water equations. *J. Comput. Phys.*, 231(15):4993–5015, 2012.

[9] C. Berthon, F. Marche, and R. Turpault. An efficient scheme on wet/dry transitions for shallow water equations with friction. *Comput. & Fluids*, 48:192–201, 2011.

[10] F. Bouchut. *Nonlinear stability of finite volume methods for hyperbolic conservation laws and well-balanced schemes for sources.* Frontiers in Mathematics. Birkhäuser Verlag, Basel, 2004.

[11] C. Chalons, F. Coquel, E. Godlewski, P.-A. Raviart, and N. Seguin. Godunov-type schemes for hyperbolic systems with parameter-dependent source. The case of Euler system with friction. *Math. Models Methods Appl. Sci.*, 20(11):2109–2166, 2010.

[12] A. Chertock, S. Cui, A. Kurganov, and T. Wu. Well-balanced positivity preserving central-upwind scheme for the shallow water system with friction terms. *Internat. J. Numer. Methods Fluids*, 78(6):355–383, 2015.

[13] S. Clain, S. Diot, and R. Loubère. A high-order finite volume method for systems of conservation laws—Multi-dimensional Optimal Order Detection (MOOD). *J. Comput. Phys.*, 230(10):4028–4050, 2011.

[14] S. Clain and J. Figueiredo. The MOOD method for the non-conservative shallow-water system. Oct 2014.

[15] O. Delestre, C. Lucas, P.-A. Ksinant, F. Darboux, C. Laguerre, T.-N.-T. Vo, F. James, and S. Cordier. SWASHES: a compilation of shallow water analytic solutions for hydraulic and environmental studies. *Internat. J. Numer. Methods Fluids*, 72(3):269–300, 2013.

[16] V. Desveaux, M. Zenk, C. Berthon, and C. Klingenberg. A well-balanced scheme for the Euler equation with a gravitational potential. In *Finite volumes for complex applications. VII. Methods and theoretical aspects*, volume 77 of *Springer Proc. Math. Stat.*, pages 217–226. Springer, Cham, 2014.

[17] E. D. Fernández-Nieto, D. Bresch, and J. Monnier. A consistent intermediate wave speed for a well-balanced HLLC solver. *C. R. Math. Acad. Sci. Paris*, 346(13-14):795–800, 2008.

[18] U. S. Fjordholm, S. Mishra, and E. Tadmor. Well-balanced and energy stable schemes for the shallow water equations with discontinuous topography. *J. Comput. Phys.*, 230(14):5587–5609, 2011.

[19] J. M. Gallardo, M. Castro, C. Parés, and J. M. González-Vida. On a well-balanced high-order finite volume scheme for the shallow water equations with bottom topography and dry areas. In *Hyperbolic problems: theory, numerics, applications*, pages 259–270. Springer, Berlin, 2008.

[20] E. Godlewski and P.-A. Raviart. *Numerical approximation of hyperbolic systems of conservation laws*, volume 118 of *Applied Mathematical Sciences*. Springer-Verlag, New York, 1996.

[21] L. Gosse. A well-balanced flux-vector splitting scheme designed for hyperbolic systems of conservation laws with source terms. *Comput. Math. Appl.*, 39(9-10):135–159, 2000.

[22] S. Gottlieb, C.-W. Shu, and E. Tadmor. Strong stability-preserving high-order time discretization methods. *SIAM Rev.*, 43(1):89–112, 2001.

[23] N. Goutal and F. Maurel. Proceedings of the 2nd Workshop on Dam-Break Wave Simulation. Technical report, Groupe Hydraulique Fluviale, Département Laboratoire National d'Hydraulique, Electricité de France, 1997.

[24] J. M. Greenberg and A. Leroux. A well-balanced scheme for the numerical processing of source terms in hyperbolic equations. *SIAM J. Numer. Anal.*, 33(1):1–16, 1996.

[25] A. Harten, P. D. Lax, and B. van Leer. On upstream differencing and Godunov-type schemes for hyperbolic conservation laws. *SIAM Rev.*, 25(1):35–61, 1983.

[26] X. Y. Hu, N. A. Adams, and C.-W. Shu. Positivity-preserving method for high-order conservative schemes solving compressible Euler equations. *J. Comput. Phys.*, 242:169–180, 2013.

[27] S. Jin. A steady-state capturing method for hyperbolic systems with geometrical source terms. *M2AN Math. Model. Numer. Anal.*, 35(4):631–645, 2001.

[28] R. Käppeli and S. Mishra. Well-balanced schemes for the Euler equations with gravitation. *J. Comput. Phys.*, 259:199–219, 2014.

[29] R. J. LeVeque. *Numerical methods for conservation laws*. Lectures in Mathematics ETH Zürich. Birkhäuser Verlag, Basel, second edition, 1992.

[30] R. J. LeVeque. *Finite volume methods for hyperbolic problems*. Cambridge Texts in Applied Mathematics. Cambridge University Press, Cambridge, 2002.

[31] Q. Liang and F. Marche. Numerical resolution of well-balanced shallow water equations with complex source terms. *Advances in Water Resources*, 32(6):873 – 884, 2009.

[32] M. Lukáčová-Medviďová, S. Noelle, and M. Kraft. Well-balanced finite volume evolution Galerkin methods for the shallow water equations. *J. Comput. Phys.*, 221(1):122–147, 2007.

[33] J. Luo, K. Xu, and N. Liu. A well-balanced symplecticity-preserving gas-kinetic scheme for hydrodynamic equations under gravitational field. *SIAM J. Sci. Comput.*, 33(5):2356–2381, 2011.

[34] R. Manning. On the flow of water in open channels and pipes. *Institution of Civil Engineers of Ireland*, 1890.

[35] V. Michel-Dansac, C. Berthon, S. Clain, and F. Foucher. A well-balanced scheme for the shallow-water equations with topography. September 2015.

[36] R. Natalini, M. Ribot, and M. Twarogowska. A well-balanced numerical scheme for a one dimensional quasilinear hyperbolic model of chemotaxis. *Commun. Math. Sci.*, 12(1):13–39, 2014.

[37] I. K. Nikolos and A. I. Delis. An unstructured node-centered finite volume scheme for shallow water flows with wet-dry fronts over complex topography. *Comput. Methods Appl. Mech. Engrg.*, 198(47-48):3723–3750, 2009.

[38] S. Noelle, Y. Xing, and C.-W. Shu. High-order well-balanced finite volume WENO schemes for shallow water equation with moving water. *J. Comput. Phys.*, 226(1):29–58, 2007.

[39] G. Russo and A. Khe. High order well balanced schemes for systems of balance laws. In *Hyperbolic problems: theory, numerics and applications*, volume 67 of *Proc. Sympos. Appl. Math.*, pages 919–928. Amer. Math. Soc., Providence, RI, 2009.

[40] E. F. Toro. *Riemann solvers and numerical methods for fluid dynamics*. Springer-Verlag, Berlin, third edition, 2009. A practical introduction.

[41] E. F. Toro, M. Spruce, and W. Speares. Restoration of the contact surface in the HLL-Riemann solver. *Shock Waves*, 4(1):25–34, 1994.

[42] B. van Leer. Towards the ultimate conservative difference scheme, V. A second order sequel to Godunov's method. *J. Com. Phys.*, 32:101–136, 1979.

[43] B. van Leer. On the relation between the upwind-differencing schemes of Godunov, Engquist-Osher and Roe. *SIAM J. Sci. Statist. Comput.*, 5(1):1–20, 1984.

[44] Y. Xing. Exactly well-balanced discontinuous Galerkin methods for the shallow water equations with moving water equilibrium. *J. Comput. Phys.*, 257(part A):536–553, 2014.

[45] Y. Xing, C.-W. Shu, and S. Noelle. On the advantage of well-balanced schemes for moving-water equilibria of the shallow water equations. *J. Sci. Comput.*, 48(1-3):339–349, 2011.

[46] K. Xu. A well-balanced gas-kinetic scheme for the shallow-water equations with source terms. *J. Comput. Phys.*, 178(2):533–562, 2002.

[47] K. Xu, J. Luo, and S. Chen. A well-balanced kinetic scheme for gas dynamic equations under gravitational field. *Adv. Appl. Math. Mech.*, 2(2):200–210, 2010.